

Dear Editor,

According to the reviewers' comments and suggestions, we have made major revision to our manuscript. The main changes in the manuscript are as follows:

- 1) As suggested by one reviewer, we add an analysis of uncertainty reduction and add a new section of "uncertainty reduction".
- 2) We reorganize Section 2.1 to further clarify the differences between GCASv1 and GCASv2.
- 3) We add more discussions about the use of 1-week assimilation window.
- 4) We added 4 sensitivity experiments for the year of 2010 to test the impact of assimilation window, spurious signals, and uncertainty in fossil fuel carbon emissions on the inverted global and regional BIO carbon fluxes.

The point-by-point response to the reviews and the detailed changes are listed in the attachments. Many thanks to you and the referees for the time and effort you expend on this paper.

Best Regards,

Sincerely yours,

Fei Jiang

Referee #1

We would like to thank the anonymous referee for his/her comprehensive review and valuable suggestions. These suggestions help us to present our results more clearly. In response, we have made changes according to the referee's suggestions and replied to all comments point by point. All the page and line number for corrections are referred to the revised manuscript, while the page and line number from original reviews are kept intact.

General comments.

Authors present estimates of regional carbon dioxide flux variability based on assimilating GOSAT satellite observations of CO₂ with ensemble-based data assimilation system. The estimated CO₂ fluxes were evaluated by comparison to indexes of climate variability, and published top-down and bottom-up estimates. The analysis of the carbon cycle variability and comparison with data on climate variability makes a strong point of the study. On the other hand, the description of the ensemble-based data assimilation system can be improved. The paper is well written and can be accepted after minor revisions addressing the review suggestions.

Detailed comments.

Lines 130-139 Suggest clarifying, what becomes a state vector to optimize, currently it is implicit. Some details emerge much later on Lines 358-366, when uncertainties are discussed.

Response: Thank you for this suggestion. In this study, the terrestrial ecosystem (BIO) and ocean (OCN) carbon fluxes are treated as state vector and optimized. Indeed, as you said, the state variables had been mentioned in two places in the article. The first place is in the section of system description, and the second is in the section of "Experimental Design". In the first place, we are introducing the current system (GCASv2) that we have improved, we set 4 state vector schemes in this system for different applications: 1) only the BIO flux is state vector; 2) both BIO and OCN fluxes are treated as state vectors; 3) the BIO, OCN and FOSSIL fluxes are optimized at the same time; and 4) only net flux is optimized. In this study, we chose to optimize both BIO and OCN, which were introduced in the section of "Experimental Design". To further clarify the state vector of this study, we added a sentence of "*In this study, the second scheme was selected.*" at the end of the 2nd paragraph in section 2.1 (see Line 178, Page 7).

Lines 232-236 The logic behind selecting 1-week data assimilation window doesn't look solid, as the other ensemble-based assimilation systems use longer window in order of 12 weeks, (Peters et al. 2005, Feng et al. 2009, Jacobson et al. 2020). The notice that there was a problem reproducing CO₂ growth rate with a longer window in Zhang et al (2015) doesn't look like a strong argument, if considered in comparison with other studies.

Response: Many thanks for this suggestion. We have added more discussions about the assimilation window, and shown the mean observation (only GOSAT XCO₂) number (Figure S2) during the study period that each grid could have within the 1 week assimilation window and the 3000 km localization scale. We also conduct a test in the year of 2010 for different DA windows (1, 2 and 4 weeks) and evaluate the posterior results using surface observations

(see Table 1). We have revised that paragraph (see Lines 303-307, Lines 309-340, Pages 11-12) as follows:

“The DA window is set to one week in GCASv2, which is the same as before. Theoretically, a longer DA window is better, because CO₂ is a stable species. The longer window, the farther CO₂ will be transported. In this way, more observation stations will sense the flux change of one area, and thus more observations can be used to optimize the flux of that place. Therefore, many previous ensemble-based assimilation systems used a longer DA window (e.g., Peters et al. 2005, Feng et al. 2009, Jacobson et al. 2020). However, the farther away, the weaker signal the stations can sense. Bruhwiler et al. (2005) clearly shown that a pulse traveling from a faraway place would contribute relatively little signal compared to recent pulses from nearby source regions. In addition, Limited by the method of EnKF, this weak signal will be masked by the method's own unphysical signal (spurious correlation), and in order to reduce this influence, we must increase the ensembles, thereby greatly increasing the computational cost. Miyazaki et al. (2011) tested the differences of 3 days and 7 days DA windows, and pointed that with a longer DA window, more observation data will be available to constrain the surface flux, but a longer window can make the effect of model error more obvious. Thus, the assimilation result can be improved as long as the observations with spurious correlations can be neglected. However, spurious correlations can be more serious with increases in the DA window, because of a limited number of ensembles. As a result, a longer window is not necessarily better than a shorter window system. To avoid the influence of spurious signals, Kang et al. (2012) used a very short DA window (6 hours) in their assimilation system (LETKF_C) and pointed out that the flux inversion with a long window (3 weeks) is not as accurate as the one obtained with a 6 h DA window, particularly in smaller-scale structures. During the development of GCASv1, Zhang et al. (2015) tested different DA windows and found that the longer the window, the larger optimized terrestrial carbon sink will be, resulting in a smaller optimized annual atmospheric CO₂ growth rate as compared to the observed rate. Considering the fact that at present, due to the release of satellite XCO₂ retrievals like GOSAT and OCO-2, the atmospheric CO₂ observations and coverages have increased significantly compared to before, which means that we do not need to extend the DA window to include more observation data now. Figure S2 shows the mean super observation (see section 2.1.1, only GOSAT XCO₂) numbers during the study period that each grid could have within the 1-week DA window and a localization scale (3000 km, see the next paragraph). In most land areas and pan-tropical waters, each grid can already have more than 3 super observations. On average, each grid over the land could has 4 super observations. Two sensitivity tests in 2010 were conducted using 2- and 4- weeks DA windows but the same localization scale, the results are shown in Table S3. When the length of DA window increases from 1 week to 4 weeks, the mean super observation number increases from 4 to 9, accordingly, the inverted global BIO flux increased from -4.16 PgC yr⁻¹ to -4.49 PgC yr⁻¹, resulting in a larger deviation of the simulated and observed atmospheric CO₂ growth rate (AGR) and larger simulation error against the surface observations. Therefore, we still use the 1-week DA window in GCASv2.”

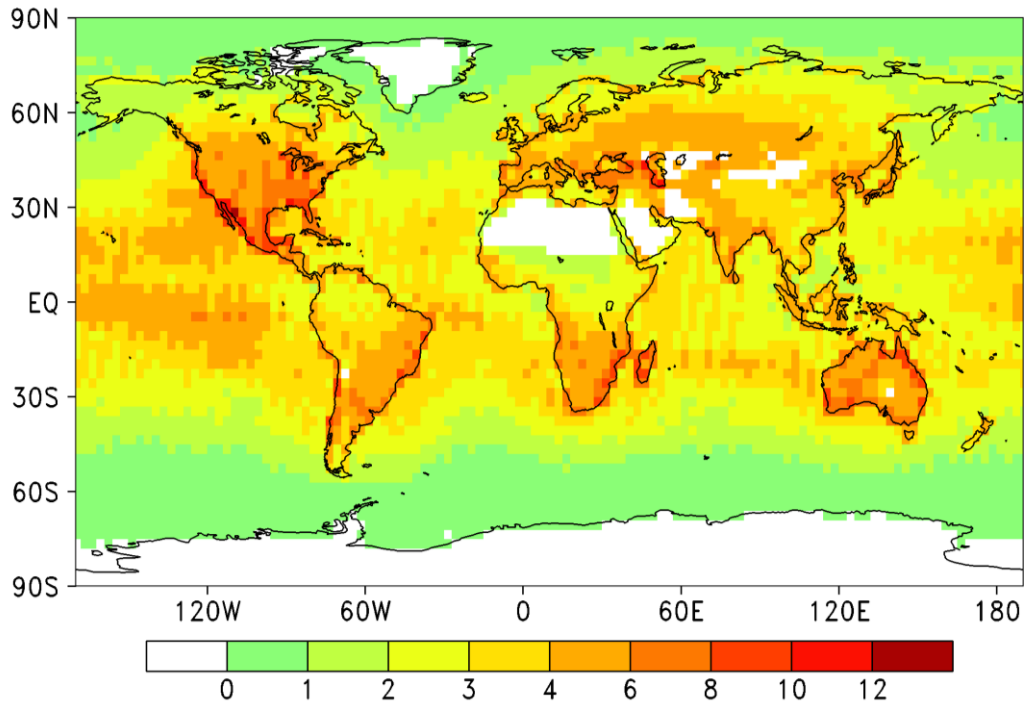


Figure 1. Mean observation numbers within a DA window (1 week) during May 2009 ~ Dec 2015 (This figure has been added in the revised Supporting Information, and named as Figure S2)

Table 1. Results of sensitivity tests in the year of 2010 (1week, 2weeks and 4weeks are three additional experiments using 1 week, 2 weeks, and 4 weeks assimilation windows, respectively) (This Table has been added in the revised Supporting Information, and named as Table S4)

		Prior	1 week	2 weeks	4 weeks
Super Obs.	Total	-	730	1039	1360
	Num. per window	Each grid over land	4	6	9
Global Flux (PgC/yr)	BIO	-2.07	-4.16	-4.46	-4.49
	OCN	-2.08	-2.33	-2.32	-2.35
	FOSSIL	9.07	9.07	9.07	9.07
	Net	7.25	4.91	4.62	4.55
Regional Flux (PgC/yr)	North America Boreal	-0.29	-0.43	-0.41	-0.35
	North America Temperate	-0.42	-1.25	-1.75	-2.41
	Tropical South America	-0.17	-0.26	-0.32	-0.27
	Temperate South America	-0.24	-0.4	-0.36	-0.19
	Northern Africa	0.21	0.32	0.36	0.62
	Southern Africa	0.22	-0.3	-0.59	-1.04
	Boreal Asia	-0.4	-0.46	-0.3	0.11
	Temperate Asia	-0.3	-0.29	-0.15	-0.06

	Southeast Asia	-0.29	-0.23	-0.21	-0.2
	Australia	-0.17	-0.4	-0.48	-0.53
	Europe	-0.19	-0.41	-0.21	-0.12
independent evaluation	BIAS	1.43	-0.44	-0.4	-0.38
	MAE	1.92	1.37	1.39	1.51
	RMSE	2.36	2.11	2.18	2.39
Deviation from the observed AGR (PgC yr ⁻¹)		2.08	-0.26	-0.55	-0.62

Technical corrections

Lines 119-120 Need to clarify, written that fluxes “are perturbed with a Gaussian random distribution” – better add more detail on whether perturbation is applied independently to each grid or over regions.

Response: Thank you! We have rewritten that sentence (see Lines 123-124, Page 5), as follows:

“the prior fluxes of X^b in each grid are independently perturbed with a Gaussian random distribution”

Line 216 As resolutions of the transport model and fluxes are apparently different, suggest writing which of them are referred as ‘model grids’.

Response: Thanks for this suggestion. We have changed ‘model grids’ as ‘transport model grids’ (see Lines 268 and 269, Page 10).

Line 584 Revise ‘a very stronger carbon sink’ as ‘a stronger carbon sink’ or ‘a very strong carbon sink’

Response: Thanks! We have changed ‘a very stronger carbon sink’ as ‘a very strong carbon sink’ (see Line 857, Page 29).

Line 594 Suggest revising ‘weak’ to ‘weaker’

Response: Thanks! We have changed ‘weak’ to ‘weaker’ (see Line 870, Page 30).

Referee #2

We thank the anonymous referee for his/her valuable comments and constructive suggestions. We have made changes according to the referee's suggestions and replied to all comments point by point. All the page and line number for corrections are referred to the revised manuscript, while the page and line number from original reviews are kept intact. The references related to the responses are listed in the end of this document.

General comments:

In this study, Jiang et al. upgraded the Global Carbon Assimilation System (GCAS) with new assimilation algorithms, a localization scheme, and a higher assimilation parameter resolution, namely GCASv2. The global terrestrial ecosystem (BIO) and ocean (OCN) carbon fluxes from 2009 to 2015 were constrained by the GOSAT ACOS XCO₂ retrievals. Following this, the posterior carbon fluxes from 2010 to 2015 were evaluated using 52 surface flask observations. The errors in the posterior carbon fluxes in the new inversion system were compared to those in a previous version. The authors indicated that the pattern of regional carbon sinks was significantly different from previous studies (CT2017). The inter-annual variations of carbon fluxes in most land regions, and the relationship with the changes of severe drought area the plant indexes, and drought were re-visited. These results are interesting. However, the improvement of the inversion methodology is not presented, and the reduction of the uncertainty by the inversions remains unclear (Figure 3) in the current paper. I, therefore, recommend that this work cannot be published before the following comments are addressed.

Specific comments:

Figure 3: What is the source for error bars in these two plots? Are they coming from the uncertainty in the prior and posterior estimates? If yes, it seems that the uncertainty is not reduced from the prior estimates to the posterior estimates. One main purpose of inversion is to reduce the uncertainty in the prior estimates. If the uncertainty is not reduced, the effectiveness of the inversions should be evaluated.

Response: Thank you for this suggestion. The error bars represent the standard deviations of all biases at each latitude and each site, respectively. Indeed, the uncertainty reduction is very important for an inversion study. We analyzed the uncertainty reduction rate (UR), and added a section of "4.2 Uncertainty reduction" in the revised manuscript (see Lines 663 – 705, Pages 21 - 23). The annual mean URs of the BIO fluxes over different TRANSCOM regions are in the range of 6% ~ 27%, with global mean of 17%. The highest monthly UR is 51% in temperate South America.

Figures 4/5: Evaluation of the reduction of the uncertainty from the prior estimates to the posterior estimates is more important than evaluation of the bias itself for an inversion system.

Response: Thank you for this suggestion. We have analyzed the reductions of the uncertainties from the prior estimates to the posterior estimates and added a section of “4.2 Uncertainty reduction” in the revised manuscript (see Lines 663 – 705, Pages 21 - 23).

Tables 2/3: What is the uncertainty for the prior and posterior estimates?

Response: Thank you! We have added the uncertainties of the prior and posterior estimates in the revised manuscript (see Lines 719 – 723, Page 24 and Line 828, Page 28).

Line 473-488: What is the uncertainty for the estimates from this study? To evaluate the effectiveness of an inversion system, the uncertainty of the posterior estimates is more important than the central value. Such information is missing in the current manuscript, which is better considered / discussed in previous studies (e.g. the literature cited in line 586).

Response: Thank you for this suggestion! As shown above, we have analyzed the uncertainty reductions and added a section of “4.2 Uncertainty reduction” in the revised manuscript (see Lines 663 – 705, Pages 21 - 23).

Figures 7/9/10: What is the uncertainty for the prior and posterior estimates?

Response: Thank you for this suggestion. We have added the prior and posterior uncertainties in Figures 7, 9 and 10, which are named as Figure 8, 10 and 11 in the revised manuscript (see Lines 893-896, Page 31; Lines 934-937, Page 33; and Lines 1045-1049, Page 37).

Figure 1: The authors suggested that a new assimilation scheme is developed in this paper. Why not directly compare the flow charts between the GCAS and GCASv2 systems and show the difference?

Response: Many thanks for this suggestion. We have modified Figure 1 and given the differences in the flow charts between GCASv1 and GCASv2 (see Lines 147-148, Page 6).

Line 124: It seems that a major advance of GCASv2 against GCAS is that “In the second step, the MOZART-4 model is run again using the optimized fluxes of X_a , to generate new CO₂ concentrations for the initial field of the next DA window. This DA flow chart is different from the previous version of GCAS, which runs the MOZART-4 model only once, and optimizes the fluxes and the initial field of the next window synchronously.” However, I do not understand how this improves the inversion system. The old GCAS system produces the posterior global gridded carbon fluxes, which were used as prior fluxes as input to any other forward models to simulate the CO₂ field. If the difference of GCASv2 was just that the posterior global gridded carbon fluxes were used by MOZART-4 to simulate the CO₂ field, I cannot see how and why the inverting methodology is improved.

Response: Thank you for this comment. Indeed, as you said, the descriptions of the differences between GCASv2 and GCASv1 are rather vague. We have revised Section 2.1 to further clarify their differences. The main differences between GCASv2 and GCASv1 are as follows:

1) Optimization of the initial field of each window. In GCASv1, it is directly optimized using the observations, while in GCASv2, it is simulated using the posterior fluxes of the previous window. The advantage of this method in GCASv2 is that the assimilation errors could be

transported from one window to the next. If the fluxes are overestimated in one window because of some reasons, by this method, they will affect the concentrations of the next window, thereby the posterior fluxes of the next window will compensate the overestimations. While in GCASv1, since the initial field of each window is directly optimized using the observations, which means in each window, there are relatively perfect initial fields, the inversions of each window are independent, and the amount of overestimation or underestimation in one window will continue to accumulate until the end, leading to an overall overestimation or underestimation. In addition, due to the perfect initial field, the differences between the simulated and observed concentrations are only contributed by the errors in the prior fluxes of current window, resulting in a relatively smaller model – data mismatch, so as to weaken the assimilation benefits on fluxes. This difference is given in Lines 128 – 143, Page 5 in the revised manuscript.

2) State vector. In GCASv1, only BIO is state vector, while in GCASv2, we set 4 state vector schemes for different applications: 1) only the BIO flux is state vector; 2) both BIO and OCN fluxes are treated as state vectors; 3) the BIO, OCN and FOSSIL fluxes are optimized at the same time; and 4) only net flux is optimized. This difference is given in Lines 172 – 178, Page 7 in the revised manuscript.

3) Resolution of the state vectors. In GCASv1, the scaling factor λ is defined in different land and ocean areas based on 22 TRANSCOM regions (Gurney et al., 2002) and 19 Olson ecosystem types, as in CarbonTracker (Peters et al., 2007), while in GCASv2, we change to use a λ in each grid, meaning that for each grid, the perturbations of prior fluxes are independent, and the grid cell of λ could be set freely. This difference is given in Lines 154-161, Page 6 in the revised manuscript.

4) observation data. In GCASv1, only flask/in situ observations were assimilated, while in GCASv2, we added a module to assimilate the satellite XCO₂ retrievals, and allow users to simultaneously or separately assimilate the flask/in situ concentrations and the XCO₂ retrievals. See Lines 186 – 201, Pages 7 -8 in the revised manuscript. Besides, a ‘super-observation’ approach is also adopted in GCASv2, See Lines 202-215, Page 8 in the revised manuscript.

5) assimilation algorithm, in GCASv2, we added another EnKF algorithm, i.e., EnSRF. See Lines 223-227, Page 9.

Line 143: It seems that the carbon emission from cement production, a large part of CO₂ source, is missed in this inversion system. This could be a big weakness of the current system. Response: Sorry, that description is not accurate enough. The carbon emission from cement production has been included in this study. The fossil fuel carbon emissions are obtained from NOAA's CarbonTracker, version CT2017, which is an average of the Carbon Dioxide Information Analysis Center (CDIAC) product (Andres et al., 2011) and the Open-source Data Inventory of Anthropogenic CO₂ (ODIAC) emission product (Oda et al., 2018). We have checked the document of CT2017 and the introduction of CDIAC database, compared the annual global fossil fuel emissions in our system with the global emissions from the CDIAC website (<https://cdiac.ess-dive.lbl.gov/>), and confirmed that the carbon emission from

cement production has been included in this study. We have changed the sentence of "... atmosphere and ocean (OCN) carbon exchange, fossil fuel (FOSSIL) carbon emission and biomass burning (FIRE) carbon emission..." to "... *atmosphere and ocean (OCN) carbon exchange, fossil fuel and cement production (FOSSIL) carbon emission and biomass burning (FIRE) carbon emission...*" (see Lines 166-167, Page 7)

Line 143: What is the relationship between BIO and FIRE? Biomass sequestrates carbon from the atmosphere, and releases CO₂ in biomass burning. Should FIRE be a part of BIO?

Response: Yes, biomass burning carbon emission is a part of terrestrial ecosystem carbon flux. Terrestrial ecosystems uptake carbon through photosynthesis (GPP) and release carbon through respiration (ER) and biomass combustion (FIRE). The BIO flux defined in this study is the net flux of GPP and ER (ER-GPP). In many previous inversion studies, it is directly defined as net ecosystem exchange [NEE = ecosystem respiration (ER) – gross primary production (GPP)] (e.g., Hu et al., 2019; Peters et al., 2007, 2010), and the sum of NEE and FIRE is defined as net biosphere exchange (NBE, Liu et al., 2017). In the revised manuscript, we have changed the sentence of "... name terrestrial ecosystem (BIO) carbon flux, ..." to "*namely terrestrial ecosystem (BIO) carbon flux (i.e., net ecosystem exchange (NEE) = ecosystem respiration (ER) – gross primary production (GPP)), ...*" (see Lines 163-166, Pages 6-7)

Line 147: "FOSSIL and FIRE fluxes are assumed to have no errors, only BIO and OCN fluxes are optimized in an assimilation system". I do not think that this is the case in other inversion systems: (1) It needs clear justification by summarizing and tabulating the methodology in the literature. (2) The difference relative to a system with errors considered for FOSSIL and FIRE need to be calculated to show how much the conclusion of the present study are sensitive to this assumption.

Response: Thank you for this comment. Yes, there are considerable uncertainties for the fossil fuel and biomass burning carbon emissions, which are about 6% and 20% for global mean, respectively. Ideally, we would like the inversion to partition the deviations from the a-priori fluxes among all the four type of carbon fluxes. NEE and ocean fluxes can, since they are geographically separated, readily be accounted for in statistically independent deviation terms. However, the inversion cannot be expected to distinguish between land biosphere fluxes and fossil fuel emissions, because both are inextricably localized on land, and the CO₂ data alone do not discern fossil and non-fossil carbon (Rödenbeck et al., 2003). Therefore, most inversion studies for surface carbon fluxes focused on the NEE and ocean fluxes, and the fossil fuel and biomass burning were prescribed (e.g., Gurney et al., 2002, 2003; Peters et al., 2007; Nassar et al., 2011; Feng et al., 2009; Monteil et al., 2020). As shown in Table 1, we have reviewed a lot of studies, in which only Deng et al. (2014, 2015) considered the uncertainties of fossil fuel and biomass burning carbon emissions, Liu et al. (2019) and Kang et al. (2012) directly optimized the net carbon flux, and Some studies (Monteil et al., 2020, Scholze et al., 2019) only optimized the NEE. Although Deng et al. (2014)'s state vector includes emissions of CO₂ from fossil fuel combustion, when they reported their posteriori flux estimates, they removed the a priori fossil fuel estimate from the reported total land flux.

As shown in section 2.1, we have added a scheme to simultaneously the fossil fuel and cement production carbon emissions in GCASv2. We have tried to use it to optimize the fossil fuel emissions in China. We tested different emission inventories, but GCASv2 did not make them converge, but only made the emissions of each inventory slightly lower. Therefore, we think that under the current resolution of atmospheric transport model, spatial coverage of observational data, and the assimilation settings, GCASv2 cannot optimize it well.

According to your suggestion, we added a sensitivity test for optimizing fossil fuel carbon emissions, using the same localization scheme as BIO and OCN, giving fossil fuels a global uncertainty of 5%. The results showed that the impact on both the inverted global and regional scale BIO fluxes are very small (Table 2).

The following sentences has been added in the revised manuscript:

“... and the FOSSIL and FIRE carbon emissions are kept intact (*the impact of this assumption on both the inverted global and regional BIO fluxes are very small (Table S4)*). Following Wang et al. (2019), ...” (see Lines 558-560, Pages 16-17)

Table 1. a summary of the inversion methodology in the literature.

System Name	Transport model/Res.	Assimilation method	Obs.	State Vector*	Reference
CT/CTE/CT-China	TM5,global 3x2, region, 1x1	EnSRF	obspack	NEE, OCN	Peters et al., 2007; Peters et al., 2010; Zhang et al., 2014
UoE	GEOS-Chem,4x5	EnKF	in situ or GOSAT	NEE, OCN	Feng et al., 2009, 2016, 2017
CAMS CO2 inversion system	LMDz,3.75x1.8 75	variational	surface observations, GOSAT, OCO-2	NEE, OCN	Chevallier, et al., 2019
CCDAS	TM3,4x5	4D-Var	in situ CO2, SM, and L-VOD	NEE	Scholze et al., 2019
Jena CarboScope	TM3,4x5	time-independent Bayesian inversion	surface observations	NBE, OCN	Rödenbeck, 2005; Rödenbeck et al., 2003
TransCom 3 inversions	16 Atmospheric Transport Models,2.0x2.5 to 7.5x7.5	Bayesian synthesis inversion	GLOBALVIEW data	NEE, OCN	Baker et al., 2006; Gurney et al., 2002, 2003

Nasser et al., 2011	GEOS-Chem, 2x2.5	time-independent Bayesian inversion	TES and surface flask measurements	NEE, OCN	Nassar et al., 2011
EUROCOM (include 6 systems)	CHIMERE, FLEXPART, STILT, TM5, NAME/0.5x0.5 ~1x1	Variational, EnKF, MCMC	flask	NEE OCN (4 prescribed)	Monteil et al., 2020
Deng et al., 2007	NIES, 2.5x2.5	Time-dependent Bayesian synthesis	GLOBALVIEW data	NEE, OCN	Deng et al., 2007
Niwa et al., 2012	NICAM-TM, ~240 km	Time-dependent Bayesian synthesis	GLOBALVIEW, CONTRAIL	NEE, OCN	Niwa et al., 2012
Miyazaki et al., 2011	AGCM, 2.8x2.8	LETKF	OSSEs (GOSAT, CONTRAIL, and surface sites)	NEE, OCN	Miyazaki et al., 2011
TM5-4DVAR inversion system	TM5, 6x4	4D-Var	GOSAT	NEE, OCN	Basu et al., 2013
GEOS-Chem-4DVAR inversion system	GEOS-Chem, 4x5	4D-Var	GOSAT, Flask	NEE, OCN, FOSSIL, FIRE	Deng et al., 2014; 2016
CMS-Flux inversion framework	GEOS-Chem, 4x5	4D-Var	GOSAT, OCO-2, SIF	NBE, OCN	Liu et al., 2017
LETKF_C	GEOS-Chem, 4x5	LETKF	OSSEs (GOSAT, CONTRAIL, and surface sites)	Net flux	Liu et al., 2019; Kang et al., 2012

*NEE: net ecosystem exchange, ecosystem respiration (ER) – gross primary production (GPP); NBE: net biosphere exchange, NEE + biomass burning carbon emission (FIRE); OCN: atmosphere - ocean carbon exchange; FOSSIL: fossil fuel and cement production carbon emission; Net flux: NEE + OCN + FOSSIL+ FIRE

Table 2. Results of sensitivity tests in the year of 2010 (Wfossil is an experiment with the

FOSSIL carbon emissions being synchronously optimized) (This Table has been added in the revised Supporting Information)

		Prior	1 week	Wfossil
Super Obs. Num. per window	Total	-	730	730
	Each grid could use	-	4	4
Global Flux (PgC/yr)	BIO	-2.07	-4.16	-4.15
	OCN	-2.08	-2.33	-2.31
	FOSSIL	9.07	9.07	9.05
	AGR	7.25	4.91	4.92
Regional Flux (PgC/yr)	North America Boreal	-0.29	-0.43	-0.44
	North America Temperate	-0.42	-1.25	-1.21
	Tropical South America	-0.17	-0.26	-0.27
	Temperate South America	-0.24	-0.4	-0.41
	Northern Africa	0.21	0.32	0.34
	Southern Africa	0.22	-0.3	-0.29
	Boreal Asia	-0.4	-0.46	-0.48
	Temperate Asia	-0.3	-0.29	-0.27
	Southeast Asia	-0.29	-0.23	-0.24
	Australia	-0.17	-0.4	-0.4
Europe	-0.19	-0.41	-0.43	
independent evaluation	BIAS	1.43	-0.44	-0.43
	MAE	1.92	1.37	1.35
	RMSE	2.36	2.11	2.08
Deviation from the observed AGR (PgC yr ⁻¹)		2.08	-0.26	-0.25

Line 209: How does GCASv2 consider the spatial representativeness errors in the inversion system?

Response: Many thanks for this question. GCASv2 do not consider the spatial representativeness errors for the GOSAT XCO₂ retrievals in this study. Generally, the spatial representation error must be considered when the resolution of the model grid is inconsistent with the spatial range represented by the observation data. In this study, we only use the XCO₂ retrievals. The reason of why we do not consider the spatial representativeness errors is that, first, the XCO₂ retrieval is a column averaged atmospheric CO₂ concentration, which is the result of full atmosphere mixing; 2) before we use the GOSAT data in GCASv2, it has been averaged within the grid cell of 1°×1°. 3) a ‘super-observation’ approach is adopted based on the optimal estimation theory (Miyazaki et al., 2012). A super-observation is generated by averaging all observations located within the same model grid within a DA window. Therefore, we believe that the spatial representation of the re-gridded and averaged XCO₂ data can match the grid of the model. In addition, the model-data mismatch error of XCO₂ is constructed using the GOSAT retrieval error, which has been uniformly inflated by a factor of 1.9 with lowest error fixed as 1 ppm. Therefore, we did not consider the spatial representation error in this study.

Line 238: How many sites are subject to this spurious noise? Are these sites excluded from the inversion system? How much does removing data at these sites influence the inversion fluxes?

Response: We have conducted an additional assimilation for the year of 2010, in which we do not remove the spurious signals, namely all the data with the correlation coefficient with the perturbed fluxes greater than zero were used for assimilation. As shown in Table 3, on average, 87% of the observations were spurious noise and removed in this study. The spurious observations will increase the inverted global land sink and enlarge the deviation of the simulated and observed atmospheric CO₂ growth rate. For different TRANSCOM regions, the impact for the BIO fluxes could be in the range of -32% to 40%. We have added the following sentences in the revised manuscript (see Lines 351-355, Page 12) and added Table 3 in the revised Supporting Information.

“...Otherwise, the relationship is assumed to be spurious noise. *On average, 87% of the observations were spurious noise and removed in this study. The spurious observations will increase the inverted global land sink and enlarge the deviation of the simulated and observed AGR. For different TRANSCOM regions, the impact for the BIO fluxes could be in the range of -32% to 40% (Table S4). The scale of 3000 km ...*”

Table 3. Results of sensitivity tests in the year of 2010 (Wnoise is the experiment with spurious signals included)

		Prior	Posterior	Wnoise
Super Obs. Num. per window	Total	-	730	730
	Each grid could use	-	4	28
Global Flux (PgC/yr)	BIO	-2.07	-4.16	-4.31
	OCN	-2.08	-2.33	-2.42
	AGR	7.25	4.91	4.67
Regional Flux (PgC/yr)	North America Boreal	-0.29	-0.43	-0.42
	North America Temperate	-0.42	-1.25	-1.41
	Tropical South America	-0.17	-0.26	-0.3
	Temperate South America	-0.24	-0.4	-0.37
	Northern Africa	0.21	0.32	0.28
	Southern Africa	0.22	-0.3	-0.42
	Boreal Asia	-0.4	-0.46	-0.33
	Temperate Asia	-0.3	-0.29	-0.31
	Southeast Asia	-0.29	-0.23	-0.27
	Australia	-0.17	-0.4	-0.4
Europe	-0.19	-0.41	-0.28	
independent evaluation	BIAS	1.43	-0.44	-0.41
	MAE	1.92	1.37	1.4
	RMSE	2.36	2.11	2.2
Deviation from the observed AGR (PgC yr ⁻¹)		2.08	-0.26	-0.5

Technical corrections:

Line 38: “BIAS” is not defined before it is used.

Response: Thanks! We have changed “BIAS” to “bias” in the revised manuscript (see Line 38, Page 2).

Line 63: “However, their carbon uptakes have significant spatial differences and interannual variations.” References are needed.

Response: Thanks for this suggestion. We have added three references, namely *Bousquet et al. (2000)*, *Takahashi et al. (2009)* and *Piao et al. (2020)*. (see Lines 65-66, Page 3)

Line 95: “However, so far, on the one hand, most studies focused on the impact of GOAST XCO 2 retrievals on the inversion of surface carbon fluxes, but in many regions, there are still large divergences for carbon sinks between different inversions with the same GOSAT data or between inversions with GOSAT and in situ observations (Chevallier et al., 2014)”. Is only one study considered and cited?

Response: Many thanks for this suggestion. We have added two references in the revised manuscript, i.e., Wang et al. (2018) and Feng et al. (2016). The sentence has been revised as follows (see Line 102, page 4 in the revised manuscript):

“...between inversions with GOSAT and in situ observations (e.g., Chevallier et al., 2014; Feng et al., 2016; Wang et al., 2018), on the other hand, ...”

Line 102. References are needed.

Response: Thank you! We have added two references, namely *Feng et al. (2017)* and *Byrne et al., (2019)*. See Line 106, Page 4 in the revised manuscript.

Line 255: The references for the two emission inventories of FOSSIL and FIRE are out of date. ODIAC and GFEDv4 have been updated recently.

Response: We have revised the reference of ODIAC “Oda and Maksyutov (2011)” as “*Oda et al. (2018)*”, and the references of GFEDv4 “van der Werf et al. (2010) and Giglio et al. (2013)” as “*Randerson et al., 2017*” (see Lines 377 and 379, Page 13)

Line 270: “The BIO carbon flux, which is the most important prior carbon flux”. Why is the prior carbon flux of BIO more important than FOSSIL and FIRE to an inversion system?

Response: This statement is problematic. From the perspective of the carbon cycle, the carbon flux of terrestrial ecosystems is not more important than others. In fact, what we want to express is that because the carbon flux of terrestrial ecosystems has the greatest uncertainty and the most significant interannual variation, when using observational data to optimize surface carbon flux, the carbon flux of terrestrial ecosystems is the most concerned. We have modified that sentence to “*The BIO carbon flux, which is one of the most concerned prior carbon fluxes in an assimilation system*” in the revised manuscript. (see Line 389, Page 13)

Line 340: When the averages of the modeled and the observational values/retrievals are equal, BIAS is zero, even if all data are distant to the 1:1 line in the comparison. BIAS cannot

effectively evaluate the performance of the model by showing how much the modeled values/retrievals agree with the observational values/retrievals. The average of absolute difference between the modeled and the observational values/retrievals is needed.

Response: Thank you! We have added the mean absolute error (MAE) between the modeled and the observational values/retrievals in the revised manuscript. (see Line 532, Page 15; Lines 577-579, Page 17; Lines 599-601, Page 18; and Lines 614 – 616, Page 19)

Line 360: Does the study of Wang et al. (2019) account for the uncertainty in FOSSIL and FIRE?

Response: No, Wang et al. (2019) only optimized the terrestrial ecosystem and ocean carbon fluxes.

Line 448: What is “impact of accumulation”?

Response: As shown in the following figure (Figure 1), we find that there is a significant increasing trend for the annual BIAS between the simulated CO₂ concentration with the posterior flux and the observed concentration. We believe that this increasing trend is due to the accumulation of errors in the assimilation system, which may be caused by the slight overestimates of land sink in each year.

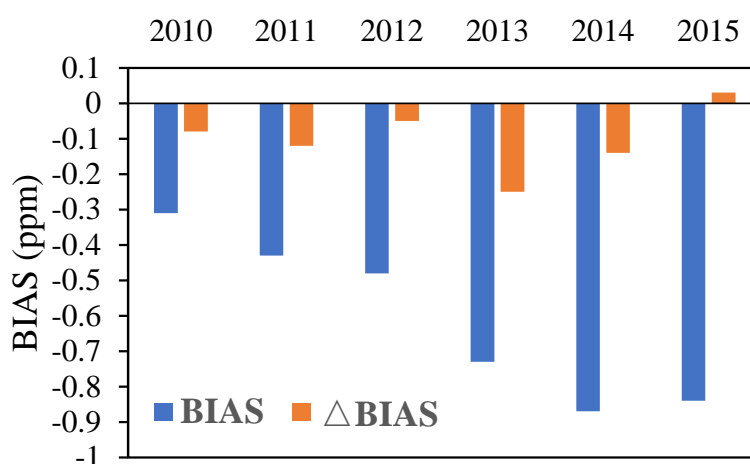


Figure 1. Annual mean BIAS between the surface flask observations and the simulations with posterior fluxes, the Δ BIAS means the difference in BIAS between two consecutive years, for example, the Δ BIAS in 2011 means the BIAS in 2011 minus the one of 2010.

Figures 3/4: “Biases” in the caption is easily confused with “BIAS” defined in equation 10.

Response: Thank you! We have modified the “Biases” in the caption Figures 3/4 to “BIAS”. (see Line 595, page 18 and Line 605, page 19)

Table 1: BIAS cannot evaluate the performance of the model by showing how much the modeled values/retrievals agree with the observed values/retrievals.

Response: Thank you for this suggestion! According to this suggestion, we have added the mean absolute error (MAE) in Table 1 in the revised manuscript. (see Line 532, Page 15; Lines 577-579, Page 17; Lines 599-601, Page 18; and Lines 614 – 616, Page 19)

Reference:

- Baker, D. F., et al.: TransCom 3 inversion intercomparison: Impact of transport model errors on the interannual variability of regional CO₂ fluxes, 1988–2003. *Global Biogeochem. Cy.*, 20, GB1002, doi:10.1029/2004GB002439, 2006.
- Basu, S., et al.: Global CO₂ fluxes estimated from GOSAT retrievals of total column CO₂, *Atmos. Chem. Phys.*, 13, 8695–8717, <https://doi.org/10.5194/acp-13-8695-2013>, 2013.
- Bousquet, P., et al.: Regional Changes in Carbon Dioxide Fluxes of Land and Oceans Since 1980, 290 (5495), 1342–1346, <https://doi.org/10.1126/science.290.5495.1342>, 2000.
- Byrne, B., et al.: On what scales can GOSAT flux inversions constrain anomalies in terrestrial ecosystems?, *Atmos. Chem. Phys.*, 19, 13017–13035, <https://doi.org/10.5194/acp-19-13017-2019>, 2019.
- Chevallier, F., et al.: Objective evaluation of surface- and satellite-driven carbon dioxide atmospheric inversions, *Atmos. Chem. Phys.*, 19, 14233–14251, <https://doi.org/10.5194/acp-19-14233-2019>, 2019.
- Deng, F., et al.: Combining GOSAT XCO₂ observations over land and ocean to improve regional CO₂ flux estimates, *J. Geophys. Res. Atmos.*, 121, 1896–1913, <https://doi.org/10.1002/2015JD024157>, 2016.
- Deng, F., et al.: Global monthly CO₂ flux inversion with focus over North America, *Tellus B*, 59, 179–190, 2007.
- Deng, F., et al.: Inferring regional sources and sinks of atmospheric CO₂ from GOSAT XCO₂ data, *Atmos. Chem. Phys.*, 14, 3703–3727, <https://doi.org/10.5194/acp-14-3703-2014>, 2014.
- Feng, L., et al.: Consistent regional fluxes of CH₄ and CO₂ inferred from GOSAT proxy XCH₄: XCO₂ retrievals, 2010–2014, *Atmos. Chem. Phys.*, 17, 4781–4797, <https://doi.org/10.5194/acp-17-4781-2017>, 2017.
- Feng, L., et al.: Estimates of European uptake of CO₂ inferred from GOSAT XCO₂ retrievals: sensitivity to measurement bias inside and outside Europe, *Atmos. Chem. Phys.*, 16, 1289–1302, <https://doi.org/10.5194/acp-16-1289-2016>, 2016.
- Feng, L., et al.: Estimating surface CO₂ fluxes from space-borne CO₂ dry air mole fraction observations using an ensemble Kalman Filter, *Atmos. Chem. Phys.*, 9, 2619–2633, <https://doi.org/10.5194/acp-9-2619-2009>, 2009.
- Gurney, K. R., et al.: Towards robust regional estimates of CO₂ sources and sinks using atmospheric transport models, *Nature*, 415, 626–630, <https://doi.org/10.1038/415626a>, 2002.
- Gurney, K. R., et al.: TransCom 3 CO₂ inversion intercomparison: 1. Annual mean control results and sensitivity to transport and prior flux information, *Tellus B*, 555–579, 2003.
- Hu, L., et al.: Enhanced North American carbon uptake associated with El Niño, *Sci. Adv.*, 5, eaaw0076, <https://doi.org/10.1126/sciadv.aaw0076>, 2019.
- Kang, J.-S., et al.: Estimation of surface carbon fluxes with an advanced data assimilation methodology, *J. Geophys. Res.*, 117, D24101, <https://doi.org/10.1029/2012JD018259>, 2012.
- Liu, J., et al.: Contrasting carbon cycle responses of the tropical continents to the 2015–2016 El Niño, *Science*, 358, eaam5690, <https://doi.org/10.1126/science.aam5690>, 2017.
- Liu, Y., et al.: Estimating surface carbon fluxes based on a local ensemble transform Kalman filter with

- a short assimilation window and a long observation window: an observing system simulation experiment test in GEOS-Chem 10.1, *Geosci. Model Dev.*, 12, 2899–2914, <https://doi.org/10.5194/gmd-12-2899-2019>, 2019.
- Miyazaki, K., et al.: Assessing the impact of satellite, aircraft, and surface observations on CO₂ flux estimation using an ensemble-based 4-D data assimilation system, *J. Geophys. Res.*, 116, D16306, <https://doi.org/10.1029/2010JD015366>, 2011.
- Monteil, G., et al.: The regional European atmospheric transport inversion comparison, EUROCOM: first results on European-wide terrestrial carbon fluxes for the period 2006–2015, *Atmos. Chem. Phys.*, 20, 12063–12091, <https://doi.org/10.5194/acp-20-12063-2020>, 2020.
- Nassar, R., et al.: Inverse modeling of CO₂ sources and sinks using satellite observations of CO₂ from TES and surface flask measurements, *Atmos. Chem. Phys.*, 11, 6029–6047, <https://doi.org/10.5194/acp-11-6029-2011>, 2011.
- Niwa, Y., et al.: Imposing strong constraints on tropical terrestrial CO₂ fluxes using passenger aircraft based measurements, *J. Geophys. Res.*, 117, D11303, doi:10.1029/2012JD017474, 2012.
- Oda, T., et al.: The Open-source Data Inventory for Anthropogenic CO₂, version 2016 (ODIAC2016): a global monthly fossil fuel CO₂ gridded emissions data product for tracer transport simulations and surface flux inversions, *Earth Syst. Sci. Data*, 10, 87–107, <https://doi.org/10.5194/essd-10-87-2018>, 2018.
- Peters, W., et al.: An atmospheric perspective on North American carbon dioxide exchange: CarbonTracker, *P. Natl. Acad. Sci.*, 104, 18925–18930, <https://doi.org/10.1073/pnas.0708986104>, 2007.
- Peters, W., et al.: Seven years of recent European net terrestrial carbon dioxide exchange constrained by atmospheric observations, *Glob. Change Biol.*, 16, 1317–1337, <https://doi.org/10.1111/j.1365-2486.2009.02078.x>, 2010.
- Piao, S., Wang, X., Wang, K., et al.: Interannual variation of terrestrial carbon cycle: Issues and perspectives, *Glob Change Biol.*, 26, 300–318, <https://doi.org/10.1111/gcb.14884>, 2020.
- Randerson, J.T., et al.: Global Fire Emissions Database, Version 4.1 (GFEDv4). ORNL DAAC, Oak Ridge, Tennessee, USA. <https://doi.org/10.3334/ORNLDAAAC/1293>, 2017.
- Rödenbeck, C., et al.: Time-dependent atmospheric CO₂ inversions based on interannually varying tracer transport. *Tellus B*, 55: 488-497. <https://doi.org/10.1034/j.1600-0889.2003.00033.x>, 2003.
- Rödenbeck, C.: Estimating CO₂ sources and sinks from atmospheric mixing ratio measurements using a global inversion of atmospheric transport, Technical Report 6, Max Planck Institute for Biogeochemistry, Jena, 2005.
- Scholze, M., et al.: Mean European carbon sink over 2010–2015 estimated by simultaneous assimilation of atmospheric CO₂, soil moisture, and vegetation optical depth. *Geophysical Research Letters*, 46, 13796–13803. <https://doi.org/10.1029/2019GL085725>, 2019.
- Takahashi, T., et al.: Climatological mean and decadal change in surface ocean pCO₂, and net sea-air CO₂ flux over the global oceans. *Deep Sea Research Part II: Topical Studies in Oceanography*, 56 (8-10): 554-577, <https://doi.org/10.1016/j.dsr2.2008.12.009>, 2009.
- Wang, J. S., et al.: A global synthesis inversion analysis of recent variability in CO₂ fluxes using GOSAT and in situ observations, *Atmos. Chem. Phys.*, 18, 11097–11124, <https://doi.org/10.5194/acp-18-11097-2018>, 2018.

Zhang, H. F. et al. Net terrestrial CO₂ exchange over China during 2001–2010 estimated with an ensemble data assimilation system for atmospheric CO₂. *J Geophys Res* 119, 3500–3515, 2014.

1
2
3
4
5
6
7
8
9
10
11
12
13
14
15
16
17
18
19
20
21
22
23
24
25
26

Regional CO₂ Fluxes during 2010-2015 Inferred from GOSAT XCO₂ retrievals using a new version of Global Carbon Assimilation System

Fei Jiang^{1,7*}, Hengmao Wang¹, Jing M. Chen², Weimin Ju¹, Xiangjun Tian³, Shuzhang Feng¹, Guicai Li⁴, Zhuoqi Chen⁵, Shupeng Zhang⁵, Xuehe Lu¹, Jane Liu^{2,6}, Haikun Wang⁶, Jun Wang¹, Wei He¹, Mousong Wu¹

- 1 Jiangsu Provincial Key Laboratory of Geographic Information Science and Technology, International Institute for Earth System Science, Nanjing University, Nanjing, 210023, China*
- 2 Department of Geography and Planning, University of Toronto, Toronto, Ontario M5S3G3, Canada*
- 3 The Institute of Atmospheric Physics, Chinese Academy of Sciences, Beijing, 100029, China*
- 4 National Satellite Meteorological Center, China Meteorological Administration, Beijing 100101, China*
- 5 College of Global Change and Earth System Science, Beijing Normal University, Beijing, 100875, China*
- 6 School of Atmospheric Sciences, Nanjing University, Nanjing, 210023, China*
- 7 Jiangsu Center for Collaborative Innovation in Geographical Information Resource Development and Application, Nanjing, 210023, China*

* Corresponding author: Tel.: +86-25-83597077; Fax: +86-25-83592288; E-mail address: jiangf@nju.edu.cn

27 **Abstract**

28 Satellite XCO₂ retrievals could help to improve carbon flux estimation because of
29 their good spatial coverage. In this study, to assimilate the GOSAT XCO₂ retrievals,
30 the Global Carbon Assimilation System (GCAS) is upgraded with new assimilation
31 algorithms, procedures and a localization scheme, a higher assimilation parameter
32 resolution and so on, and hence is named as GCASv2. Based on this new system, the
33 global terrestrial ecosystem (BIO) and ocean (OCN) carbon fluxes from May 1, 2009
34 to Dec 31, 2015 are constrained using the GOSAT ACOS XCO₂ retrievals (Version 7.3).
35 The posterior carbon fluxes from 2010 to 2015 are independently evaluated using CO₂
36 observations from 52 surface flask sites. The results show that the posterior carbon
37 fluxes could significantly improve the modeling of atmospheric CO₂ concentrations,
38 with global mean bias decreases from a prior value of 1.6 ± 1.8 ppm to -0.5 ± 1.8 ppm.
39 The uncertainty reduction (UR) of the global BIO flux is 17%, and the highest monthly
40 regional UR could reach 51%. Globally, the mean annual BIO and OCN carbon sinks
41 and their interannual variations inferred in this study are very close to the estimates of
42 CT2017 during the study period, and the inferred mean atmospheric CO₂ growth rate
43 and its interannual changes are also very close to the observations. Regionally, over the
44 northern lands, there are the strongest carbon sinks in North America Temperate,
45 followed by Europe, Boreal Asia, and Temperate Asia; and in tropics, there are strong
46 sinks in Tropical South America and Tropical Asia, but a very weak sink in Africa. This
47 pattern is significantly different from the estimates of CT2017, but the estimated carbon
48 sinks in each continent and some key regions like Boreal Asia and Amazon are
49 comparable or in the range of previous bottom-up estimates. The inversion also changes
50 the interannual variations of carbon fluxes in most TRANSCOM land regions, which
51 have a better relationship with the changes of severe drought area or LAI, or are more
52 consistent with previous estimates for the impact of drought. These results suggest that
53 the GCASv2 system works well with the GOSAT XCO₂ retrievals, and has a good
54 performance in estimating the surface carbon fluxes, meanwhile, our results also
55 indicate that the GOSAT XCO₂ retrievals could help to better understand the

删除了: BIAS

57 interannual variations of regional carbon fluxes.

58 **1. Introduction**

59 Atmospheric carbon dioxide (CO₂) is one of the most important greenhouse gases,
60 and fossil fuel burning and land use change are mostly responsible for its increase from
61 the preindustrial concentration. Terrestrial ecosystems and oceans play very important
62 roles in regulating the atmospheric CO₂ concentration. In the past half century, about
63 60% of the anthropogenic CO₂ emissions have been absorbed by the terrestrial
64 ecosystems and oceans (IPCC, 2014). However, their carbon uptakes have significant
65 spatial differences and inter-annual variations ([Bousquet et al., 2000](#); [Takahashi et al.,
66 2009](#); [Piao et al., 2020](#)). Therefore, it is very important to quantify the global and
67 regional carbon fluxes.

68 Atmospheric inversion is an effective method for estimating the surface CO₂ fluxes
69 using the globally distributed atmospheric CO₂ concentration observations (Enting and
70 Newsam, 1990; Gurney et al., 2002). It has robust performance on global or hemisphere
71 scale carbon budget estimates (Houweling et al., 2015), but on regional scales, due to
72 the uneven distribution of in situ observations, the reliability of inversion results varies
73 greatly in different regions. Generally, the inversions have large uncertainties in tropics,
74 southern hemisphere oceans and most continental interiors such as South America,
75 Africa, and Boreal Asia (Peylin et al., 2013). Satellite observation has a better spatial
76 coverage, especially over remote regions, and studies show that it can be used to
77 improve the carbon flux estimates (e.g., Chevallier et al., 2007; Miller et al., 2007;
78 Hungershofer et al., 2010). The Greenhouse Gases Observing Satellite (GOSAT)
79 (Kuze et al., 2009), being the first satellite mission dedicated to observing CO₂ from
80 space, was launched in 2009. Many inversions have utilized the GOSAT retrievals for
81 column-averaged dry air mole fractions of CO₂ (XCO₂) to infer surface carbon fluxes
82 (e.g., Basu et al., 2013; Maksyutov et al., 2013; Saeeki et al., 2013a; Chevallier et al.,
83 2014; Deng et al., 2014; Deng et al., 2016; Wang et al., 2018a; Wang et al., 2019). Takagi
84 et al. (2011) found that GOSAT XCO₂ retrievals could significantly reduce the
85 uncertainties in estimates of surface CO₂ fluxes for regions in Africa, South America,

86 and Asia, where the sparsity of the surface monitoring sites is most evident. Basu et al.
87 (2013) shown that assimilating only GOSAT data can well reproduce the observed CO₂
88 time series at the surface and TCCON sites in the tropics and the northern extra-tropics,
89 but enhance seasonal cycle amplitudes in the southern extra-tropics. Wang et al. (2019)
90 also showed that GOSAT XCO₂ retrievals can effectively improve carbon flux
91 estimation, and the performance of the inversion with GOSAT data only was
92 comparable with the one using in situ observations. Meanwhile, based on the inversions
93 with GOSAT XCO₂ retrievals, Liu et al. (2018) quantified the impacts of the 2011 and
94 2012 droughts on terrestrial ecosystem carbon uptake anomalies over the contiguous
95 US, Deng et al. (2016) compared the distributions of drought and posterior carbon
96 fluxes in South America for 2010-2012, Detmers et al. (2015) studied the impact of the
97 strong La Niña episode on the carbon fluxes in Australia from the end of 2010 to early
98 2012. However, so far, on the one hand, most studies focused on the impact of GOSAT
99 XCO₂ retrievals on the inversion of surface carbon fluxes, but in many regions, there
100 are still large divergences for carbon sinks between different inversions with the same
101 GOSAT data or between inversions with GOSAT and in situ observations ([e.g.](#),
102 [Chevallier et al., 2014](#); [Feng et al., 2016](#); [Wang et al., 2018a](#)), on the other hand,
103 although some studies reported the impact of drought or extreme wetness on the
104 changes of carbon fluxes using inversions based on GOSAT, few studies have
105 comprehensively investigated the impacts of GOSAT data on the interannual variations
106 of inverted land sinks in different regions ([Feng et al., 2017](#); [Byrne et al., 2019](#)).

107 In this study, we present a 6-year inversion from 2010 to 2015 for the global and
108 regional carbon fluxes using only the GOSAT XCO₂ retrievals. The Global Carbon
109 Assimilation System (GCAS) is employed to conduct this inversion, which was
110 developed in China in 2015 (Zhang et al., 2015) and updated in this study with a new
111 scheme to assimilate XCO₂ retrievals. The inverted multi-year averaged carbon fluxes
112 for the globe, global land and ocean, each TRANSCOM region ([Gurney et al., 2002](#)) as
113 well as some key areas are shown and compared with previous top-down and bottom-
114 up (Jiang et al., 2016) estimates. The estimated interannual variations of carbon fluxes

115 in each TRANSCOM region are given and discussed against changes in drought and
116 LAI. This manuscript is organized as follows: Section 2 details the GCASv2 system as
117 well as the prior fluxes, GOSAT retrievals and uncertainty settings. Section 3 briefly
118 introduces the experimental design. Results and discussions are presented in Section 4,
119 and Conclusions are given in Section 5.

120 2. Method and Data

121 2.1 A new version of the Global Carbon Assimilation System (GCASv2)

122 Figure 1 shows the flow chart of the GCASv2 system. In each data assimilation
123 (DA) window, there are two steps. The first step, the prior fluxes of X^b in each grid
124 are independently perturbed with a Gaussian random distribution, and put into the
125 global atmospheric chemical transport model MOZART-4 to simulate CO₂
126 concentrations, which are then sampled according to the locations and times of CO₂
127 observations. The sampled data are used in the assimilation module together with the
128 CO₂ observations to generate the optimized fluxes of X^a . In the second step, the
129 MOZART-4 model is run again using the optimized fluxes of X^a , to generate new CO₂
130 concentrations for the initial field of the next DA window. By this method, if the flux
131 in one window is overestimated because of some reasons, it will affect the
132 concentrations of the next window, thereby the posterior flux of the next window will
133 compensate the overestimation. This DA flow chart is different from the previous
134 version of GCAS (GCASv1), which runs the MOZART-4 model only once, and
135 optimizes the fluxes and the initial field of the next window synchronously. namely in
136 each window, there is relatively perfect initial field (directly optimized using
137 observations), the inversions of each window are independent, and the amount of
138 overestimation or underestimation in one window will continue to accumulate until the
139 end, leading to an overall overestimation or underestimation. In addition, due to the
140 relatively perfect initial field, the differences between the simulated and observed
141 concentrations are only contributed by the errors in the prior fluxes of current window,
142 resulting in a relatively smaller model – data mismatch, so as to weaken the assimilation
143 benefits on fluxes.

删除了:.

删除了: In this study, we find the synchronous dual optimizations will weaken the assimilation benefits on fluxes.

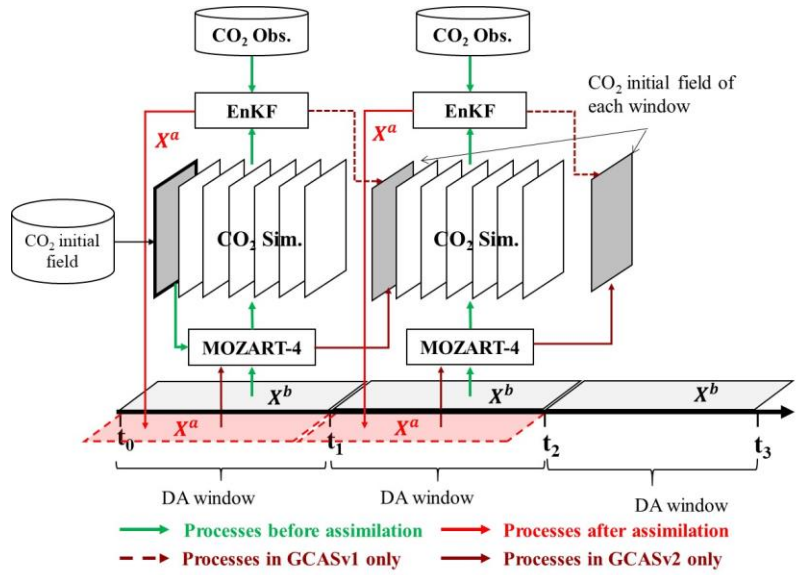


Figure 1. Flow chart of the GCASv2 system

The perturbation of X^b represents the uncertainty of the prior carbon flux, which is calculated using the following function.

$$X_i^b = X_0^b + \lambda \times \delta_i \times X_0^b, i = 1, 2, \dots, N \quad (1)$$

where δ_i represents random perturbation samples, which is drawn from Gaussian distributions with mean zero and standard deviation of one. N is the ensemble size. λ is a set of scaling factors, which represents the uncertainty of each prior flux. In GCASv1, λ is defined in different land and ocean areas based on 22 TRANSCOM regions (Gurney et al., 2002) and 19 Olson ecosystem types, as in CarbonTracker (CT, Peters et al., 2007). This means that in the same area, the error of a prior flux is the same. Through assimilation, the flux will be integrally enlarged or reduced. In GCASv2, we change to use a λ in each grid, meaning that for each grid, the perturbations of prior fluxes are independent. In addition, the grid cell of λ is different from those of the prior flux and the transport model, which could be set freely. X_0^b is prior carbon flux. Generally, there are 4 types of carbon fluxes, namely terrestrial ecosystem (BIO) carbon flux (i.e., net ecosystem exchange (NEE) = ecosystem respiration (ER) - gross primary

删除了: previous version GCAS

删除了: terrestrial ecosystem

166 production (GPP), atmosphere and ocean (OCN) carbon exchange, fossil fuel and
 167 cement production (FOSSIL) carbon emission and biomass burning (FIRE) carbon
 168 emission, which are used to drive the transport model to simulate the atmospheric CO₂
 169 concentration. And in general, FOSSIL and FIRE fluxes are assumed to have no errors,
 170 only BIO and OCN fluxes are optimized in an assimilation system (e.g., Gurney et al.,
 171 2002; Peters, et al., 2007; Nassar et al., 2011; Jiang et al., 2013; Chevallier, et al., 2019).
 172 In GCASv1, only the BIO flux was treated as state vector and optimized, the OCN flux
 173 was directly from the output of CarbonTraker (CT). In GCASv2, it is set to be an
 174 optional item. Four schemes are set (Functions 2 - 5). The first one is the same as the
 175 previous version, only the BIO flux is optimized; the second one is the same as general,
 176 namely both BIO and OCN fluxes are state vectors; the third one is that BIO, OCN and
 177 FOSSIL fluxes are optimized at the same time; and the fourth one is that only net flux
 178 is optimized. In this study, the second scheme was selected.

删除了: carbon flux

删除了: Wang et al., 2019

删除了: optimized

$$179 \quad X_i^b = (X_{bio}^b + \lambda_{bio} \times \delta_{i,bio} \times X_{bio}^b) + X_{ocn}^b + X_{fossil}^b + X_{fire}^b, i = 1, 2, \dots, N \quad (2)$$

$$180 \quad X_i^b = (X_{bio}^b + \lambda_{bio} \times \delta_{i,bio} \times X_{bio}^b) + (X_{ocn}^b + \lambda_{ocn} \times \delta_{i,ocn} \times X_{ocn}^b) \\ 181 \quad + X_{fossil}^b + X_{fire}^b, i = 1, 2, \dots, N \quad (3)$$

$$182 \quad X_i^b = (X_{bio}^b + \lambda_{bio} \times \delta_{i,bio} \times X_{bio}^b) + (X_{ocn}^b + \lambda_{ocn} \times \delta_{i,ocn} \times X_{ocn}^b) \\ 183 \quad + (X_{fossil}^b + \lambda_{fossil} \times \delta_{i,fossil} \times X_{fossil}^b) + X_{fire}^b, i = 1, 2, \dots, N \quad (4)$$

$$184 \quad X_i^b = (X_{bio}^b + X_{ocn}^b + X_{fossil}^b + X_{fire}^b) + \lambda_{netflux} \times \delta_{i,netflux} \times (X_{bio}^b + \\ 185 \quad X_{ocn}^b + X_{fossil}^b + X_{fire}^b), i = 1, 2, \dots, N \quad (5)$$

186 For the CO₂ observations, in GCASv1, only the flask and in situ observations were
 187 assimilated. In GCASv2, we added a module to use satellite XCO₂ retrievals. With this
 188 module, simulated CO₂ concentration profiles are converted to XCO₂ concentrations,
 189 and users can choose to assimilate flask/in situ observations or satellite XCO₂ retrievals
 190 alone, or simultaneously assimilate these two data. The simulated CO₂ concentration

移动了(插入) [2]

删除了: For the modeled XCO₂, the

设置了格式: 下标

设置了格式: 下标

profiles are mapped into the satellite retrieval levels and then vertically integrated based on satellite averaging kernel according to the following equation (Connor, et al., 2008),

$$XCO_2^m = XCO_2^a + \sum_j h_j a_j (A(x) - y_{a,j}) \quad (6)$$

where j denotes the retrieval level; x is the simulated CO_2 profile, and $A(x)$ is a mapping matrix; XCO_2^a is the prior XCO_2 ; h_j is a pressure weighting function, a_j and $y_{a,j}$ are the satellite column averaging kernel and the prior CO_2 profile for retrieval, respectively.

To reduce the computational cost and the influence of representative errors, a 'super-observation' approach is also adopted in GCASv2 based on the optimal estimation theory (Miyazaki et al., 2012). A super-observation is generated by averaging all observations located within the same model grid within a DA window. We assume that the observation errors of different stations at different times are independent of each other. The standard deviation of the j th observation y_j is r_j . The super-observation y_{new} , standard deviation r_{new} and corresponding simulations $x_{new,i}$ from one perturbed prior flux X_i^b are calculated:

$$1/r_{new}^2 = \sum_{j=1}^m 1/r_j^2 \quad (7)$$

$$y_{new} = \sum_{j=1}^m w_j y_j / \sum_{j=1}^m w_j \quad (8)$$

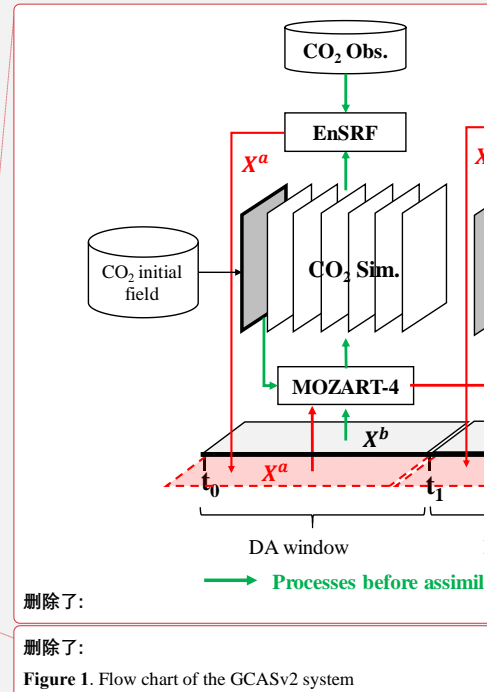
$$x_{new,i} = \sum_{j=1}^m w_j x_{j,i} / \sum_{j=1}^m w_j \quad (9)$$

where $w_j = 1/r_j^2$ is the weighting factor; m is the number of observations within a super-observation grid. The super-observation error decreases as the number of observations used for the super-observation increases.

2.1.1 EnSRF assimilation algorithm

删除了: should be first

删除了: 10



223 Besides the Local Ensemble Transform Kalman Filter (LETKF), which has been
 224 implemented in GCASv1, to avoid storing and inverting very large matrices during
 225 analysis, in GCASv2, we added another assimilation algorithm, namely the Ensemble
 226 square root filter (EnSRF) algorithm (Whitaker and Hamill, 2002), which has been
 227 successfully used in CT (Peters et al., 2005). EnSRF obviates the need to perturb the
 228 observations in contrast to the traditional EnKF algorithm and assimilates observations
 229 in a sequential way. It has a better performance than the method to assimilate
 230 observations simultaneously as long as the observation errors are uncorrelated
 231 (Houtekamer and Mitchell, 2001). The implementation process and setup are detailed
 232 below.

删除了: introduced by Whitaker and Hamill (2002),

删除了: is used to constrain the carbon fluxes in this version

233 After obtaining an ensemble of state vectors as described in Section 2.1, ensemble
 234 runs of MOZART-4 are conducted to propagate these errors in the model with each
 235 ensemble sample of a state vector. The background error covariance \mathbf{P}^b is calculated
 236 based on the forecast ensemble from Eq. (7):

删除了: 6

$$237 \quad \mathbf{P}^b = \frac{1}{n-1} \sum_{i=1}^n (\mathbf{X}_i^b - \bar{\mathbf{X}}^b) (\mathbf{X}_i^b - \bar{\mathbf{X}}^b)^T \quad (10)$$

删除了: 6

238 where $\bar{\mathbf{X}}^b$ represents the mean of the ensemble samples. Based on the background
 239 error covariance, the response of the uncertainty in the simulated concentrations to the
 240 uncertainty in emissions is obtained. Combing observational vector \mathbf{y} , the state vector
 241 is updated according to the following formulations:

$$242 \quad \bar{\mathbf{X}}^a = \bar{\mathbf{X}}^b + \mathbf{K}(\mathbf{y} - \mathbf{H}\bar{\mathbf{X}}^b) \quad (11)$$

删除了: 7

$$243 \quad \mathbf{K} = \mathbf{P}^b \mathbf{H}^T (\mathbf{H} \mathbf{P}^b \mathbf{H}^T + \mathbf{R})^{-1} \quad (12)$$

删除了: 8

$$244 \quad \delta \mathbf{X}_i^a = \delta \mathbf{X}_i^b - \tilde{\mathbf{K}} \mathbf{H} \delta \mathbf{X}_i^b \quad (13)$$

删除了: 9

245 While employing sequential assimilation and independent observations

$$246 \quad \tilde{\mathbf{K}} = (1 + \sqrt{\mathbf{R} / \mathbf{H} \mathbf{P}^b \mathbf{H}^T + \mathbf{R}})^{-1} \mathbf{K} \quad (14)$$

删除了: 0

247 where \mathbf{H} is the observation operator that maps the state variable from model space to

256 observation space. \mathbf{K} is the Kalman gain matrix of ensemble mean depending on
 257 background and observation error covariance \mathbf{R} , representing the relative contributions
 258 to analysis. $\tilde{\mathbf{K}}$ is the Kalman gain matrix of ensemble perturbation, and then emission
 259 perturbations after inversion $\delta\mathbf{X}_i^a$ can be calculated. At the analysis step, the ensemble
 260 mean $\overline{\mathbf{X}^a}$ is taken as the best estimate of the carbon flux.

261 2.1.2 Atmospheric transport model

262 Same as the [GCASv1](#) (Zhang et al., 2015), the global chemical transport Model for
 263 OZone And Related chemical Tracers (MOZART-4; Emmons et al., 2010) is adopted
 264 as the atmospheric transport model in GCASv2. MOZART-4 is a flexible model, it can
 265 be run at essentially any resolution, and can be driven by essentially any meteorological
 266 data set and with any emission inventories (Emmons et al., 2010). In this system, we
 267 preset two horizontal resolutions for MOZART runs, one being approximately
 268 $2.8^\circ \times 2.8^\circ$, with [transport model grids](#) of 128×64 , and another being approximately
 269 $1.0^\circ \times 1.0^\circ$, with [the model grids](#) of 360×180 . In the vertical direction, we use 28 layers.
 270 The ERA-Interim reanalysis datasets from the European Centre for Medium-Range
 271 Weather Forecasts (ECMWF) are used to drive the model. ERA-Interim data set
 272 includes as many as 128 meteorological variables, and has the highest spatial resolution
 273 of approximately 80 km (T255 spectral) on 60 vertical levels from the surface up to 0.1
 274 hPa. Only the variables required for MOZART-4 with a spatial resolution of $1.0^\circ \times 1.0^\circ$,
 275 and 28 vertical levels for 3-D variables from the surface to approximately 2.5 hPa are
 276 selected in this system. The selected variables and vertical levels are shown in Table S1
 277 and S2 in the supporting information.

278 2.1.3 DA window and localization

279 The DA window is set to one week in GCASv2, which is the same as before.
 280 Theoretically, a longer DA window is better, because CO_2 is a stable species. The longer
 281 window, the farther CO_2 will be transported. In this way, more observation stations will
 282 sense the flux change of one area, and thus more observations can be used to optimize
 283 the flux of that place. [Therefore, many previous ensemble-based assimilation systems](#)

删除了:

To reduce the computational cost and the influence of representative errors, a 'super-observation' approach is adopted based on the optimal estimation theory (Miyazaki et al., 2012). A super-observation is generated by averaging all observations located within the same model grid within a DA window. We assume that the observation errors of different stations at different times are independent of each other. The standard deviation of the j th observation y_j is r_j . The super-observation y_{new} , standard deviation r_{new} and corresponding simulations $x_{new,i}$ from one perturbed prior flux X_i^p are calculated:

$$1/r_{new}^2 = \sum_{j=1}^m 1/r_j^2 \quad (7)$$

$$y_{new} = \sum_{j=1}^m w_j y_j / \sum_{j=1}^m w_j \quad (8)$$

$$x_{new,i} = \sum_{j=1}^m w_j x_{j,i} / \sum_{j=1}^m w_j \quad (9)$$

where $w_j = 1/r_j^2$ is the weighting factor; m is the number of observations within a super-observation grid. The super-observation error decreases as the number of observations used for the super-observation increases.

删除了: GCAS system

304 used a longer DA window (e.g., Peters et al. 2005, Feng et al. 2009, Jacobson et al.
305 2020). However, the farther away, the weaker signal the stations can sense. Bruhwiler
306 et al. (2005) clearly shown that a pulse traveling from a faraway place would contribute
307 relatively little signal compared to recent pulses from nearby source regions. In addition,
308 Limited by the method of EnKF, this weak signal will be masked by the method's own
309 unphysical signal (spurious correlation), and in order to reduce this influence, we must
310 increase the ensembles, thereby greatly increasing the computational cost. Miyazaki et
311 al. (2011) tested the differences of 3 days and 7 days DA windows, and pointed that
312 with a longer DA window, more observation data will be available to constrain the
313 surface flux, but a longer window can make the effect of model error more obvious.
314 Thus, the assimilation result can be improved as long as the observations with spurious
315 correlations can be neglected. However, spurious correlations can be more serious with
316 increases in the DA window, because of a limited number of ensembles. As a result, a
317 longer window is not necessarily better than a shorter window system. To avoid the
318 influence of spurious signals, Kang et al. (2012) used a very short DA window (6 hours)
319 in their assimilation system (LETKF_C) and pointed out that the flux inversion with a
320 long window (3 weeks) is not as accurate as the one obtained with a 6 h DA window,
321 particularly in smaller-scale structures. During the development of GCASv1, Zhang et
322 al. (2015) tested different DA windows and found that the longer the window, the larger
323 optimized terrestrial carbon sink will be, resulting in a smaller optimized annual
324 atmospheric CO₂ growth rate (AGR) as compared to the observed rate. Considering the
325 fact that at present, due to the release of satellite XCO₂ retrievals like GOSAT and OCO-
326 2, the atmospheric CO₂ observations and coverages have increased significantly
327 compared to before, which means that we do not need to extend the DA window to
328 include more observation data now. Figure S2 shows the mean super observation (see
329 section 2.1.1, only GOSAT XCO₂) numbers during the study period that each grid
330 (3°×3°) could have within a 1-week DA window and a localization scale (3000 km, see
331 the next paragraph). In most land areas and pan-tropical waters, each grid can already
332 have more than 3 super observations. On average, each grid over the land could has 4

333 super observations. Two sensitivity tests in 2010 were conducted in this study using 2-
334 and 4-weeks DA windows but a same localization scale, the results are shown in Table
335 S4. When the length of DA window increases from 1 week to 4 weeks, the mean super
336 observation number increases from 4 to 9, accordingly, the inverted global BIO flux
337 increased from -4.16 PgC yr⁻¹ to -4.49 PgC yr⁻¹, resulting in a larger deviation of the
338 simulated and observed AGR and larger simulation error against the surface
339 observations. Therefore, we still use the 1-week DA window in GCASv2.

340 As discussed before, in the EnKF method, there are inevitably spurious correlations.
341 Therefore, a localization scale, which determines that only measurements located
342 within a certain distance (cutoff radius) from a grid point will influence the analysis of
343 this grid, must be set to reduce the effect of spurious correlations. The localization
344 technique in this study is based on both the distance between one site and one grid cell
345 of λ , and the linear correlation coefficient between the simulated concentrations and the
346 perturbed fluxes for each parameter (λ)/observation pair. If the distance is less than 500
347 km and the correlation coefficient is greater than zero, the observations will be accepted
348 for assimilation, and if the distance is greater than/equal to 500 km and less than 3000
349 km and the relationship between a parameter deviation and its modeled observational
350 impact is statistically significant ($p < 0.05$), then that relationship is retained. Otherwise,
351 the relationship is assumed to be spurious noise. On average, 87% of the observations
352 were spurious noise and removed in this study. The spurious observations will increase
353 the inverted global land sink and enlarge the deviation of the simulated and observed
354 AGR. For different TRANSCOM regions, the impact for the inverted BIO fluxes could
355 be in the range of -32% to 40% (Table S4). The scale of 3000 km is set simply according
356 to the globally-averaged 80-m wind speed during the day (4.96 m/s, Archer and
357 Jacobson, 2005) and the length of DA window (1 week).

358 2.2 Prior carbon fluxes

359 As described in Section 2.1, there are 4 types of prior carbon fluxes in GCASv2.
360 In this study, FOSSIL carbon emissions are obtained from NOAA's CT, version 2017
361 (CT2017, Peters et al. 2007, with updates documented at <http://carbontracker.noaa.gov>),

删除了:

In addition, Zhang et al. (2015) tested different DA window lengths and found that the longer the window, the larger optimized terrestrial carbon sink will be, resulting in a smaller optimized annual atmospheric CO₂ growth rate as compared to the observed rate. Therefore, they pointed out that the 1-week DA window seems to be most suitable. For this reason, this study also uses the same DA window of one week as before. ...

删除了: I

删除了: arbon

删除了: racker

删除了: CT

375 which is an average of the Carbon Dioxide Information Analysis Center (CDIAC)
376 product (Andres et al., 2011) and the Open-source Data Inventory of Anthropogenic
377 CO₂ (ODIAC) emission product (Oda et al., 2018). The FIRE CO₂ emissions are also
378 taken from CT2017, which are the average of the Global Fire Emissions Database
379 version 4.1 (GFEDv4) (Randerson et al., 2017) and the Global Fire Emission Database
380 from the NASA Carbon Monitoring System (GFED_CMS). The OCN CO₂ exchange
381 is from the pCO₂-Clim prior of CT2017, which is derived from the Takahashi et al.
382 (2009) climatology of seawater pCO₂. In addition, as shown in Figure 7 of the
383 CarbonTracker Documentation CT2017 release ([https://www.esrl.noaa.gov/gmd/ccgg/
384 carbontracker/CT2017/](https://www.esrl.noaa.gov/gmd/ccgg/carbontracker/CT2017/), accessed on 4 Mar, 2020), there are no data in many seas like
385 Japan Sea, Mediterranean, Gulf of Mexico, East China Sea, and so on, and therefore,
386 the fluxes in 2009 modeled using the global ocean circulation (OPA) and the
387 biogeochemistry model (PISCES-T) (Buitenhuis et al., 2006; Jiang et al., 2013) is used
388 to fill the no data areas.

删除了: Oda and Maksyutov, 2011

删除了: van der Werf et al., 2010; Giglio et al., 2013

389 The BIO carbon flux, which is one of the most concerned prior carbon fluxes in an
390 assimilation system, was simulated using the Boreal Ecosystems Productivity
391 Simulator (BEPS) model (Chen et al., 1999; Ju et al., 2006) in this study. BEPS is a
392 process-based, remote sensing data driven, and mechanistic ecosystem model. In this
393 study, BEPS model was run starting from 2000. To simplify the initialization, the initial
394 values of the different carbon pools are from a previous BEPS simulation (Chen et al.,
395 2019). In short, all carbon pools were assumed to be in a state of dynamic equilibrium
396 from 1901 to 1910. And all carbon pools were determined by solving a set of equations
397 describing the dynamics of carbon pools (Chen et al., 2003). Then the simulation
398 forwarded using historical data. Due to the lack of historical data of remote sensed LAI
399 data, the averaged LAI from 1982 to 1986 represented that over the 1901-1981 period.
400 Then, all our initial carbon pools were set to states of carbon pools in 2000 according
401 to Chen et al. (2019). The BEPS model was also driven by the 1°×1° ERA-Interim
402 reanalysis datasets, including relative humidity, wind speed, air temperature, incoming
403 solar radiation, and total precipitation. The other data include LAI data and clumping

删除了: important

407 index. LAI was inverted from surface reflectance datasets of Moderate Resolution
 408 Imaging Spectroradiometer (MODIS) (Liu et al., 2012), and the clumping index was
 409 derived from the MODIS Bidirectional Reflectance Distribution Function (BRDF)
 410 products, which provided the finest pseudo multi-angular data for the land surface,
 411 according to Normalized Difference between Hotspot and Darkspot (NDHD) (Chen et
 412 al., 2005, He et al., 2012).

413 2.3 GOSAT XCO₂ retrievals

414 The GOSAT XCO₂ retrievals of the ACOS Version 7.3 Level 2 Lite product
 415 (O'Dell et al., 2012; Crisp et al., 2012) at the pixel level during May 2009 ~ Dec 2015
 416 is used in this study, which is bias-corrected (Wunch et al., 2011). In order to achieve
 417 the most extensive spatial coverage with the assurance of using best quality data
 418 available, before being used in the inversion system, the XCO₂ retrievals are filtered
 419 with two parameters of warn_levels and xco2_quality_flag, which are provided along
 420 with the product. Only the data with xco2_quality_flag greater than 0 are selected. The
 421 selected data are then divided into three groups according the value of warn_levels, that
 422 are with warn_levels less than 8, greater than 9 and less than 12, and greater than 13,
 423 respectively. The group with smallest warn_levels has the best data quality, while that
 424 with the largest is the worst. Then, the pixel data are averaged within the grid cell of
 425 1°×1°, and in each grid, only the group with best data quality is selected and then
 426 averaged. The other variables like column-averaging kernel, retrieval error and so on
 427 which are provided along with the XCO₂ product are also dealt with the same method.
 428 This process is the same as Wang et al. (2019). Except the XCO₂, the other quantities,
 429 provided along with the ACOS product were also filtered and averaged to 1°×1° grid
 430 according to the above method.

431 2.4 Evaluation data and method

432 Generally, direct validation of the optimized flux is impossible, and instead, we
 433 indirectly evaluate the posterior flux by comparing the forward simulated atmospheric
 434 CO₂ mixing ratios against measurements (e.g., Jin et al., 2018; Wang et al., 2019; Feng

带格式的: 段落间距段后: 1 行

移动了(插入) [1]

删除了: simulated

删除了: profile

删除了: are

删除了: and

删除了:

上移了 [2]: For the modeled XCO₂, the simulated CO₂ concentration profile should be first mapped into the satellite retrieval levels and then vertically integrated according to the following equation.

$$XCO_2^m = XCO_2^a + \sum_j h_j a_j (A(x) - y_{a,j})$$

(10)

where j denotes the retrieval level; x is the simulated CO₂ profile, and $A(x)$ is a mapping matrix; XCO_2^a is the prior XCO₂; h_j is a pressure weighting function, a_j and $y_{a,j}$ are the satellite column averaging kernel and the prior CO₂ profile for retrieval, respectively. Except the simulated CO₂ profile,

删除了: For the modeled XCO₂, the simulated CO₂ concentration profile should be first mapped into the satellite retrieval levels and then vertically integrated according to the following equation.

$$XCO_2^m = XCO_2^a + \sum_j h_j a_j (A(x) - y_{a,j})$$

(10)

where j denotes the retrieval level; x is the simulated CO₂ profile, and $A(x)$ is a mapping matrix; XCO_2^a is the prior XCO₂; h_j is a pressure weighting function, a_j and $y_{a,j}$ are the satellite column averaging kernel and the prior CO₂ profile for retrieval, respectively. Except the simulated CO₂ profile, the other quantities are provided along with the ACOS product and filtered and averaged to 1°×1° grid according to the above method.

带格式的: 段落间距段前: 0 磅, 段后: 0 磅

删除了: where j denotes the retrieval level; x is the simulated profile, and $A(x)$ is a mapping matrix; XCO_2^a is the prior XCO₂; h_j is a pressure weighting function, a_j and $y_{a,j}$ are the satellite column averaging kernel and the prior CO₂ profile for retrieval, respectively. Except the simulated CO₂ profile, the other quantities are provided along with the ACOS

上移了 [1]: Except the simulated CO₂ profile, the other quantities are provided along with the ACOS product and filtered and averaged to 1°×1° grid according to the above

511 et al., 2020). First, the simulated XCO₂ are compared against the corresponding GOSAT
 512 XCO₂ retrievals to test the effectiveness of the assimilation system (see Section 2.3 for
 513 the description of the GOSAT XCO₂ retrieval). Second, Surface CO₂ observations used
 514 for independent evaluations in this study are obtained from the
 515 obspack_co2_1_GLOBALVIEWplus_v5.0_2019-08-12 product. It is a subset of the
 516 Observation Package (ObsPack) Data Product (ObsPack, 2019), and contains a
 517 collection of discrete and quasi-continuous measurements at surface, tower and ship
 518 sites contributed by national and universities laboratories around the world. In this study,
 519 surface CO₂ measurements from 52 flask sites are selected to evaluate the posterior CO₂
 520 concentrations, which are all provided by the NOAA Global Monitoring Laboratory
 521 (with lab number of 1 in each filename). The locations of the 52 sites could be found in
 522 Figure 2 and the corresponding sites code as well as the information latitude and
 523 longitude are listed in Table S3 in the Supporting Information.

524 During the evaluation, 4 basic statistical measures, namely mean bias (BIAS),
 525 mean absolute error (MAE), root mean square error (RMSE), and correlation
 526 coefficient (CORR), are calculated against the surface CO₂ observations and GOSAT
 527 XCO₂ retrievals, respectively. The BIAS, MAE, RMSE, and CORR reflect the overall
 528 model tendency, both the model bias and error variance, and the linear correspondence
 529 between the modeled and observational values/retrievals, respectively. The functions of
 530 these 4 basic statistical measures are expressed as:

$$531 \quad BIAS = \frac{1}{M} \sum_{j=1}^M (x_j - y_j) = \bar{y} - \bar{x} \quad (15)$$

$$532 \quad MAE = \frac{1}{M} \sum_{j=1}^M |x_j - y_j| \quad (16)$$

$$533 \quad RMSE = \sqrt{\frac{1}{M} \sum_{j=1}^M (x_j - y_j)^2} \quad (17)$$

$$534 \quad CORR = \frac{\sum_{j=1}^M (x_j - \bar{x})(y_j - \bar{y})}{\sqrt{\sum_{j=1}^M (x_j - \bar{x})^2} \sqrt{\sum_{j=1}^M (y_j - \bar{y})^2}} \quad (18)$$

535 where x_j and y_j denote the modeled and the observational values/retrievals,

删除了: 3

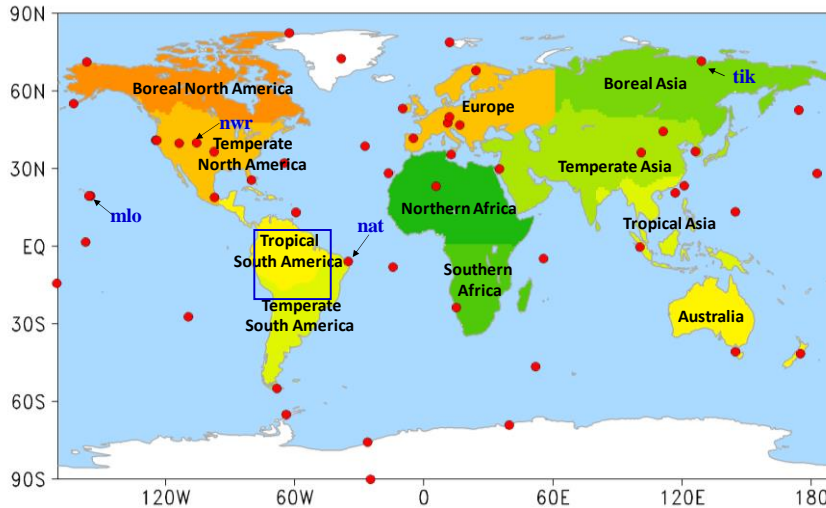
删除了: 3

删除了: 0

删除了: 11

删除了: 12

541 respectively, at the j th out of M records, and the overbars denote averages.



542 **Figure 2.** Distributions of the observation sites used in this study. Red solid circles are
543 the 52 surface flask sites used for evaluations, the shaded shows the 11 TRANSCOM
544 regions, the blue rectangle shows the Amazon region, which is defined the same as
545 Botta et al. (2012)
546

547 3. Experimental Design

548 The assimilation system was run from May 1, 2009 to Dec 31, 2015. Two forward
549 simulations with the prior and posterior fluxes were also conducted from May 1, 2009
550 to Dec 31, 2015, respectively. For both assimilation and forward runs, the initial field
551 of 3-D CO₂ concentrations at 00:00 UTC May 1, 2009 was from the product of CT2017
552 as well, and the MOZART-4 model was run with the resolution of 2.8°×2.8°. The first
553 8 months are considered as a spin-up run, and the results from Jan 1, 2010 to Dec 31,
554 2015 are analyzed and evaluated in this study.

555 During the assimilation, the resolution of λ is the same as the transport model. For
556 the state vector, the second scheme (Function 3) was adopted, namely the BIO CO₂
557 exchanges and OCN fluxes are optimized in this study, and the FOSSIL and FIRE
558 carbon emissions are kept intact (the impact of this assumption on both the inverted

删除了..

560 global and regional BIO fluxes are very small (Table S4). Following Wang et al.
561 (2019), global annual uncertainties of 100% and 40% are assigned to BIO and OCN
562 CO₂ exchanges, respectively. Accordingly, the uncertainties of the scaling factor (λ)
563 for the prior BIO and OCN fluxes in each DA window at the grid cell level are assigned
564 to 3 and 5, respectively. The model-data mismatch error of XCO₂ is constructed using
565 the GOSAT retrieval error, which is provided along with the ACOS product. According
566 to the previous works of Wang et al. (2019) and Deng et al. (2014), all retrieval errors
567 are also uniformly inflated by a factor of 1.9 in this study, which is the same as Wang
568 et al. (2019), but a lowest error is added in this study, which is fixed as 1 ppm.

569 4. Results and Discussions

570 4.1 Evaluation for the inversion results

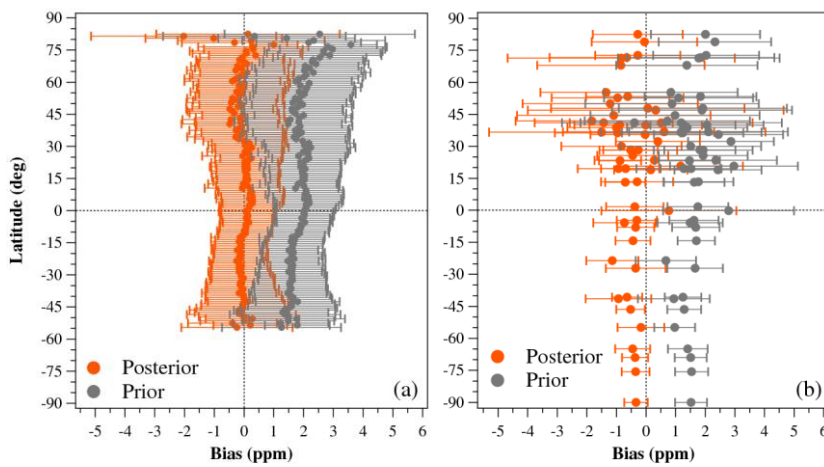
571 4.1.1 Evaluation using assimilated GOSAT XCO₂ retrievals

572 Figure 3a shows the zonal mean XCO₂ model-data mismatch errors at different
573 latitudes during the study period. Compared with the GOSAT XCO₂ retrievals, basically
574 all the zonal mean BIAS of the prior XCO₂ in different latitudes are greater than 1 ppm,
575 with a global mean of 1.8 ± 1.3 ppm (average \pm standard deviation), but for the posterior
576 XCO₂, most zonal average BIAS are within ± 0.5 ppm, with global mean of -0.0 ± 1.1
577 ppm. The global mean MAE and RMSE between the simulated and GOSAT retrieved
578 XCO₂ concentrations also decreases from a prior value of 2.0 and 2.2 ppm to 0.8 and
579 1.1 ppm, respectively (Table 1), indicating that the model-data mismatch errors between
580 the simulated and retrieved XCO₂ are significantly reduced. Overall, for both prior and
581 posterior concentrations, the BIAS in the southern hemisphere is smaller than that in
582 the northern hemisphere. In the same hemisphere, the BIAS at low latitudes is smaller
583 than that at high latitudes. Figure 4 shows the spatial distribution of the posterior XCO₂
584 biases. It could be found that in most grids (~80%), the biases are within ± 1 ppm. In
585 Tropical Pacific, North Pacific, North Atlantic and Tropical Land, most biases are
586 positive, and in the northern extra-tropical lands, negative biases are dominant. This

删除了: A

删除了: , same thereafter

589 pattern may be related to the retrieval errors, and the large BIAS in the high latitudes
 590 may be attributed to the large retrieval errors in those areas, which are caused by the
 591 lower solar elevation angle. Overall, this small posterior BIAS, which is less than the
 592 retrieval error (Crisp et al., 2012), indicates that the GCASv2 system works well with
 593 the GOSAT XCO₂ retrievals in this study.



594
 595 **Figure 3.** BIAS at different latitudes (a, simulated and retrieved XCO₂; b, simulated
 596 and observed CO₂ mixing ratios; error bar represents the standard deviations of the
 597 biases at each latitude and each site, respectively)

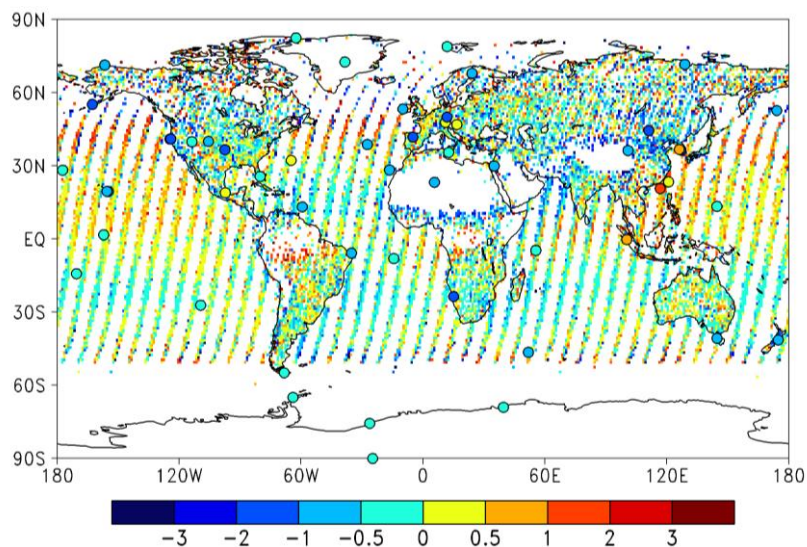
删除了: Biases

598
 599 **Table1.** Statistics of the simulated surface CO₂ and XCO₂ concentrations against the
 600 surface flask observations and GOSAT retrievals, respectively

	BIAS		MAE		RMSE		CORR	
	Prior	Post.	Prior	Post.	Prior	Post.	Prior	Post.
XCO ₂	1.8±1.3	-0.0±1.1	2.0	0.8	2.2	1.1	0.95	0.96
Surface CO ₂	1.6±1.8	-0.5±1.8	2.1	1.4	2.4	1.9	0.96	0.96

601 *mean ± standard deviation

602



604
605 **Figure 4.** Distributions of the **BIAS** of the posterior (cycle) surface CO₂ and (grid
606 shaded) XCO₂ concentrations (simulations minus observations/retrievals)

删除了: mean biases

607 4.1.2 Evaluation using independent surface observations

608 Figure 3b shows the mean biases of the simulated surface CO₂ mixing ratios at each
609 flask site at different latitudes. It could be found that the BIAS of the prior CO₂ mixing
610 ratios are basically greater than 1 ppm at different latitudes, with global mean of 1.6±1.8
611 ppm, after constraining using the GOSAT XCO₂ retrievals, the BIAS at most sites are
612 within ±1 ppm, with a global mean of -0.5±1.8 ppm. These BIAS are similar to those
613 of Basu et al. (2013), in which the average model–observation bias decreased from a
614 prior value of 1.95 ppm to -0.55 ppm. The MAE and RMSE between the simulated and
615 surface flask concentrations are also reduced in most sites, with the global mean MAE
616 and RMSE decreasing from 2.1 and 2.4 to 1.4 and 1.9 ppm, respectively (Table 1). The
617 BIAS in the northern hemisphere are significantly larger than those in southern
618 hemisphere, because the carbon flux in the northern hemisphere is more complex than
619 that of the southern hemisphere (Wang et al., 2019). In addition, the posterior BIAS in
620 most sites are negative, especially in the middle latitudes in the northern hemisphere.
621 The significant negative biases (less than 1 ppm) are mainly distributed in North

删除了: In our study,

删除了: t

625 America, Europe, central Asia, while positive biases are mainly located along east
626 Asian coast (Figure 4), indicating that the carbon sinks in North America and Europe
627 might be overestimated in this study, while those in the upwind areas of east Asian
628 coastal sites, mainly eastern China, may be underestimated.

629 Moreover, it also could be found that the global mean prior BIAS of XCO₂ (about
630 1.8 ppm) is greater than the surface concentrations (1.6 ppm), while the BIAS of XCO₂
631 reduced by inversion (about 1.8 ppm) is less than the reduction of BIAS in the surface
632 concentrations (about 2.1 ppm). This may be attributed to the fact that, on the one hand,
633 although the GOSAT XCO₂ retrievals were bias-corrected, there may still be some
634 systematic deviations; on the other hand, the responses of surface observations to
635 changes in the surface carbon flux is faster than the XCO₂ concentrations, so that larger
636 flux adjustments are needed to match XCO₂ concentration with ground data. A similar
637 situation was reported in Wang et al. (2019). In their study, GOSAT XCO₂ retrievals
638 were used to optimize the terrestrial carbon flux in 2015. Their inversion reduced the
639 BIAS of simulated surface and XCO₂ (compared against TCCON sites) concentrations
640 by about 1.1 and 0.9 ppm, respectively.

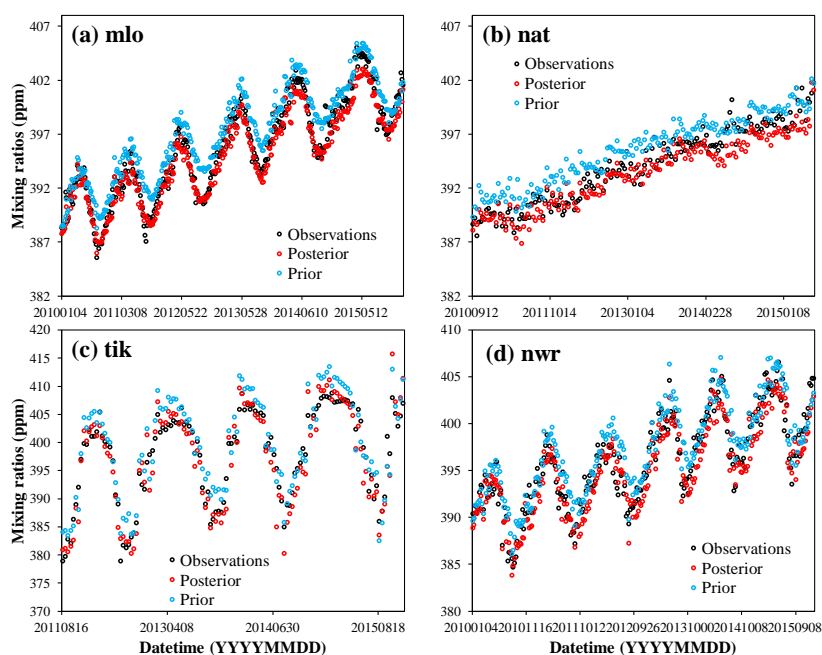
641 Figure 5 shows the time series of simulated and observed CO₂ mixing ratios at four
642 sites, i.e., mlo, nwr, tik, and nat. The mlo and nwr sites are two mountain stations located
643 in the center of Pacific and western US, respectively, and nat and tik are two coastal
644 sites located in Amazon and Siberia, respectively (Figure 2). Overall, the posterior
645 mixing ratios have a better agreement with the observations at all 4 sites. The mlo site
646 is an atmospheric baseline station. At mlo, the posterior mixing ratio well reproduces
647 the observed concentration, while the prior concentrations are overestimated all the
648 time since the summer of 2010, especially during the summertime every year. Besides,
649 the posterior concentrations during the wintertime are underestimated, and the
650 underestimation gradually increases along with time. A similar situation also could be
651 found at the nat site as well as other sites located in tropical and southern hemisphere
652 oceans (Figure not shown). Figure S1 shows the interannual variations of the global
653 mean BIAS. Clearly, the biases of surface CO₂ are gradually accumulated, leading to

删除了: 2

删除了: 0

656 the relatively large mean bias (-0.5 ppm). If we remove the impact of accumulation, the
 657 annual BIAS is about -0.1 ppm per year (about -0.2 PgC yr⁻¹). There are no error
 658 accumulations at most land sites like nwr and tik. These indicate that the global net
 659 carbon sinks are slightly overestimated every year, but in different lands, there are
 660 interannual variations.

删除了: bias



661
 662 **Figure 5.** Modeled and observed CO₂ time series at four surface stations

663 **4.2 Uncertainty reduction**

664 The uncertainty reduction rate (UR) is another important quantity to evaluate the
 665 performance of GCASv2 and the effectiveness of GOSAT XCO₂ retrievals in this
 666 system (Chevallier et al., 2007; Takagi et al., 2011). Following Chevallier et al. (2007),
 667 the UR is defined as

668
$$UR = \left(1 - \frac{\sigma_{posterior}}{\sigma_{prior}}\right) \times 100 \quad (19)$$

670 where $\sigma_{posterior}$ and σ_{prior} are the posterior and prior uncertainties, respectively.
671 The URs on regional carbon flux estimates vary significantly over time and space (Deng
672 et al., 2014; Takagi et al., 2011). Table 2 lists the annual mean 1- σ URs relative to the
673 prior uncertainties during 2010 ~ 2015, which were aggregated in the 22 TRANSCOM
674 regions and 4 large-scale regions. It shows that over land regions, the annual mean URs
675 are in the range of 6% ~ 27%. The regions with large UR are temperate South America,
676 southern Africa, temperate North America, Europe. The UR over tropical and boreal
677 regions are relatively small due to the lower spatial coverage of XCO₂. This distribution
678 is similar to the results of Deng et al. (2014), which are mainly related to the spatial
679 coverage of GOSAT XCO₂. For the monthly UR, in high latitudes, there are high URs
680 in the warm season and very low ones in cold seasons; in mid-latitudes, the UR is
681 significant throughout the year; and in tropical areas, it is related to the rainy season. In
682 the rainy season, the URs are very low due to the massive cloud coverage, while in the
683 dry season, the monthly UR are significant, with the highest UR reaching 25%. Figure
684 6 shows the monthly uncertainties in temperate North America and Europe. It could be
685 found that in Europe, high URs are mainly during May ~ September, and in temperate
686 North America, there are high URs in each month, with the highest UR reaching 45%.
687 The highest monthly UR is in temperate South America, with value of 50%. The highest
688 monthly and annual URs are lower than the ones given in previous studies (40%–70%,
689 Takagi et al., 2011; Deng et al., 2014; Saeki et al., 2013a), which may be related to the
690 grided state vector and shorter DA window used in this study.

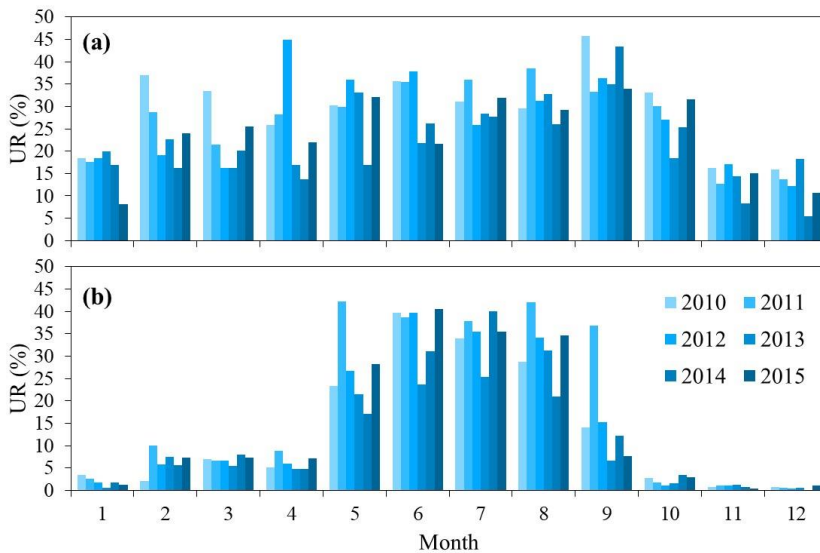
691 Over the ocean regions, the URs are very low, with values in the range of 0.12% ~
692 3.7%. As shown in formula (14), the UR is mainly determined by the observation
693 uncertainty R and background error covariance P^b (prior uncertainty). Usually, a small
694 R and large P^b corresponds to a large UR, and vice versa. Since we used a scheme in
695 which the prior uncertainties were proportional to the prior fluxes, thereby the regions
696 with small prior fluxes would have small prior uncertainties and small URs. Compared
697 to those over the lands, there are much weaker fluxes and much larger XCO₂
698 uncertainties (Wunch et al., 2017) over the oceans, resulting in the significantly lower

699 URs over the oceans. Previous studies (e.g., Takagi et al., 2011; Kadygrov et al., 2009)
 700 also showed very low URs over the oceans.

701 **Table 2.** Annual mean prior uncertainties and reduction rates (UR) aggregated in
 702 different TRANSCOM Regions during 2010~2015

<u>Region</u>	<u>Prior Unc.</u> <u>(PgC yr⁻¹)</u>	<u>UR</u> <u>(%)</u>	<u>Region</u>	<u>Prior Unc.</u> <u>(PgC yr⁻¹)</u>	<u>UR</u> <u>(%)</u>
<u>Boreal North America</u>	0.82	7.8	<u>North Pacific</u>	0.49	0.29
<u>Temperate North America</u>	1.62	26.4	<u>West Pacific</u>	0.15	0.47
<u>Tropical South America</u>	1.28	6.4	<u>East Pacific</u>	0.42	3.71
<u>Temperate South America</u>	1.27	27.2	<u>South Pacific</u>	0.33	0.42
<u>Northern Africa</u>	1.5	5.9	<u>Arctic Ocean</u>	0.30	0.14
<u>Southern Africa</u>	1.35	15.9	<u>North Atlantic</u>	0.27	0.17
<u>Boreal Asia</u>	1.24	15.6	<u>Tropical Atlantic</u>	0.13	0.60
<u>Temperate Asia</u>	1.23	10.3	<u>South Atlantic</u>	0.25	0.46
<u>Tropical Asia</u>	0.77	8.0	<u>Southern Ocean</u>	0.40	0.12
<u>Australia</u>	0.50	10.0	<u>North Indian Ocean</u>	0.17	0.43
<u>Europe</u>	1.31	19.8	<u>South Indian Ocean</u>	0.35	0.33
<u>Northern Lands</u>	2.91	19.9	<u>Northern Oceans</u>	0.65	0.13
<u>Tropical Lands</u>	2.57	9.0	<u>Tropical Oceans</u>	0.51	2.82
<u>Southern Lands</u>	1.38	24.4	<u>Southern Oceans</u>	0.68	0.27
<u>Global Lands</u>	4.24	17.1	<u>Global Oceans</u>	1.11	0.84

703



704

705 **Figure 6.** Monthly uncertainties in (a) temperate North America and (b) Europe

706 **4.3 Global Carbon Budget**

707 Table 3 presents the mean prior and posterior global carbon budgets during 2010 ~
 708 2015 of this study. For comparison, the mean global carbon budgets from Global
 709 Carbon Budget 2018 (GCP2018, Le Quéré et al., 2018), CT2017, and Jena CarboScope
 710 (JCS, Rödenbeck, 2005) are also shown. Both CT2017 and JCS estimates of the
 711 surface-atmosphere CO₂ exchange were based on the atmospheric measurements of
 712 CO₂ concentrations. In this study, the JCS product of s04oc_v4.3 is adopted. It should
 713 to be noted that JCS only provides the net biosphere exchange (NBE), which is the sum
 714 of BIO carbon flux and FIRE carbon emissions, and no individual FIRE carbon
 715 emissions data is available. To compare, the FIRE carbon emissions used in this study,
 716 which is from CT2017, is also applied to the JCS data, namely the BIO carbon flux of
 717 JCS in this manuscript is obtained from the NBE of JCS minus the FIRE carbon
 718 emission of this study.

719 **Table 3.** Mean global carbon budgets during 2010 ~2015 estimated in this study as well
 720 as those from the prior fluxes, GCP2018, CT2017 and JCS (PgC yr⁻¹)

	Prior	Posterior	GCP2018	CT2017	JCS
Fossil fuel and industry (FOSSIL)	9.58	9.58	9.49	9.62	9.31
Biomass burning (FIRE)	2.02	2.02	1.52*	2.03	2.02
Terrestrial ecosystem (BIO)	-4.07 _{+4.24}	-4.24 _{+3.51}	-3.13	-4.29	-4.07
Ocean (OCN)	-2.47 _{+1.11}	-2.56 _{+1.10}	-2.46	-2.57	-2.25
Budget imbalance	-	-	-0.52	-	-
Net biosphere exchange <u>(NBE)</u> ***	-2.05 _{+4.24}	-2.22 _{+3.51}	-2.12	-2.27	-2.05
Global net carbon flux (AGR)	5.06 _{+4.38}	4.80 _{+3.67}	4.91**	4.79	5.01

721 * land-use change emissions, **atmospheric growth in GCP2018, *** for GCP2018, it
 722 is the sum of BIO, FIRE and budget imbalance, and for the others, it is the sum of BIO
 723 flux and FIRE emission.

724 The mean posterior BIO carbon flux during 2010-2015 in this study is -4.24_{+3.51}
 725 PgC yr⁻¹ (negative/positive mean carbon uptake/release from/to the atmosphere, same
 726 thereafter), and the OCN flux is -2.56_{+1.10} PgC yr⁻¹, after considering the FOSSIL

删除了: 2

删除了: 2

删除了: land-atmosphere carbon flux

删除了: land-atmosphere carbon flux

删除了:

删除了: 2

733 carbon emission (9.58 PgC yr⁻¹) and FIRE carbon emission (2.02 PgC yr⁻¹), the mean
734 global net carbon flux (i.e., atmospheric CO₂ growth rate) inverted in this study is
735 4.80±3.67 PgC yr⁻¹. Both the posterior BIO and OCN carbon fluxes are stronger than
736 the prior ones, and the posterior global net carbon flux is weaker than the prior one.
737 Compared with the others, both posterior BIO and OCN fluxes are close to the ones of
738 CT2017, but higher than the ones of JCS. The AGR of GCP2018 was estimated directly
739 from atmospheric CO₂ measurements, which were provided by the US National
740 Oceanic and Atmospheric Administration Earth System Research Laboratory
741 (NOAA/ESRL) (Dlugokencky and Tans, 2018), and therefore, it could be considered
742 as a true value. The posterior AGR in this study (4.8 PgC yr⁻¹) is slightly lower than
743 GCP2018 and very close to CT2017. Compared with GCP2018, the deviations of prior
744 and JCS AGR are 0.15 and 0.10 PgC yr⁻¹, while the ones of posterior and CT2017 are
745 -0.11 and -0.12 PgC yr⁻¹, respectively.

删除了: atmospheric CO₂ growth rate (

删除了:)

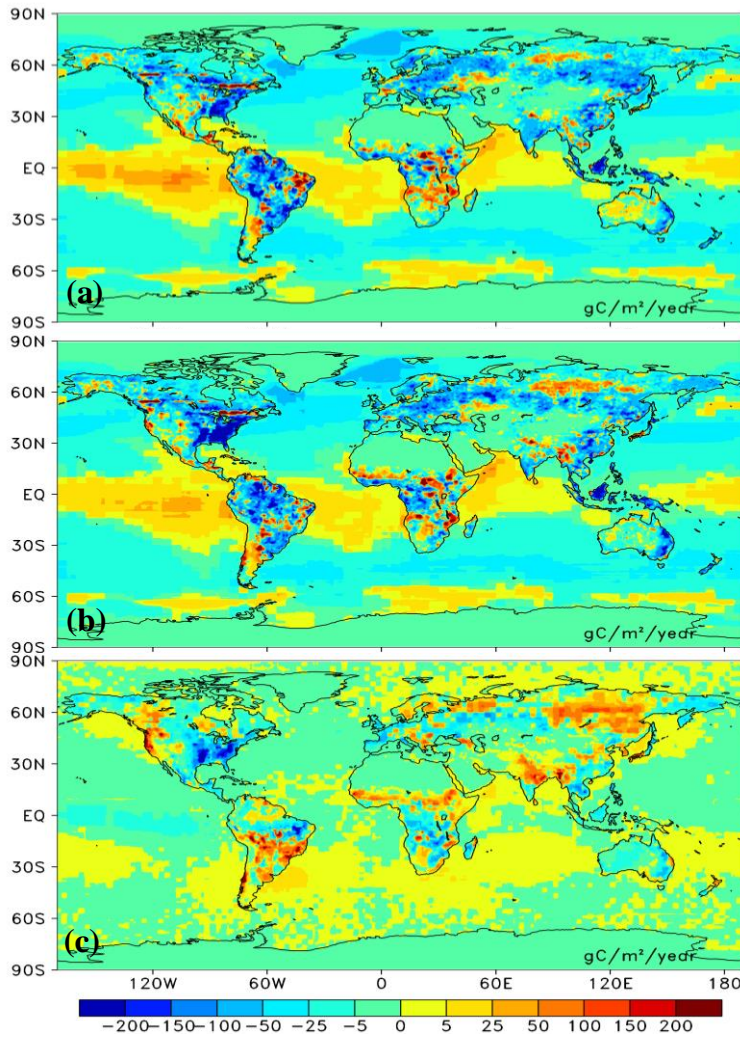
746 4.4 Regional Carbon Flux

747 Figure 7 shows the distributions of the mean prior and posterior annual BIO and
748 OCN carbon fluxes as well as their differences during 2010 - 2015. For the prior BIO
749 flux, carbon uptakes mainly occur over eastern North America, Amazon, southern
750 Brazil, western Europe, southern Russia, eastern China, South Asia and Malay
751 Archipelago; and carbon releases mainly occur in western North America, eastern
752 Amazon, Argentina, most Africa, Indo-China Peninsula, and parts of eastern Europe
753 and Russia. For the prior OCN flux, carbon uptakes mainly happen in mid-latitude
754 regions in both hemispheres, while carbon sources are mainly in tropical oceans and
755 Southern Ocean. After the constraint with the GOSAT XCO₂ retrievals, the overall
756 patterns of carbon sinks and sources are similar to the prior ones. However, the BIO
757 sinks in East and Central America, eastern Amazon, tropical Africa, Indo-China
758 Peninsula, and southwestern Russia are obviously increased, on the contrary, in western
759 North America, temperate South America, extra-tropical Africa, South Asia, Southwest
760 China, North China, Siberia, and parts of southern and northern Europe, the carbon

删除了: 3

删除了: 6

765 sources are increased. For the OCN flux, in most tropical and northern hemisphere
 766 oceans, the carbon sinks are slightly increased, while in most southern hemisphere
 767 oceans, the carbon sources are slightly enhanced.



768
 769 **Figure 7.** Distributions of mean annual terrestrial ecosystem and ocean carbon fluxes
 770 (a, prior; b, posterior and c, their differences (posterior - prior), unit: $\text{gC m}^{-2}\text{yr}^{-1}$)
 771 Table 4 lists the aggregated mean annual prior and posterior BIO carbon fluxes
 772 during 2010-2015 for the 11 TRANSCOM land regions (Figure 2, Gurney et al., 2002)

删除了: 6
 删除了:)
 删除了: and
 删除了:)
 删除了:)
 删除了: (
 删除了: 3

780 as well as 3 aggregated large-scale regions, i.e., Northern Lands, Tropical Lands, and
781 Southern Lands. Northern lands include Boreal North America, Temperate North
782 America, Boreal Asia, Temperate Asia and Europe; Tropical Lands include Tropical
783 South America, Tropical Asia, Northern Africa and Southern Africa; and Southern
784 Lands include Temperate South America and Australia. For the prior, there is a largest
785 carbon sink in Tropical South America, followed by Boreal Asia and Temperate Asia,
786 and a weakest carbon flux in Southern Africa. After optimization using GOSAT XCO₂
787 retrievals, the carbon sinks of Temperate North America, Southern Africa are
788 significantly increased, and those in Australia and Europe are also enhanced. However,
789 in Temperate South America, Northern Africa, Boreal Asia, and Temperate Asia, the
790 carbon sinks are decreased. Very small changes are found in Boreal North America,
791 Tropical South America, and Tropical Asia, especially for Tropical South America,
792 however, as shown in Figure 7, there are obvious changes over different areas in
793 Tropical South America, thus the zero change in statistics in this region may be just a
794 coincidence. For the Amazon region (Figure 2), the estimated BIO flux is decreased
795 from a prior of -0.52 ± 1.46 PgC yr⁻¹ to -0.45 ± 1.28 PgC yr⁻¹. The largest carbon sink
796 occurs in Temperate North America, followed by Tropical South America and Europe,
797 and the weakest sink appears in Northern Africa.

删除了: 6

798 For comparisons, Table 4 also lists the mean BIO carbon fluxes of CT2017 and
799 JCS for the same period. For the 3 large-scale regions, i.e., Northern Lands, Tropical
800 Lands and Southern Lands, the same as the global total BIO carbon sink, the carbon
801 sinks in these 3 regions are also similar to CT2017. However, in each region, the
802 distributions of carbon sinks between this study and CT2017 are significantly different.
803 In Northern Lands, the carbon sinks estimated by this study are more evenly distributed,
804 although Temperate North America has the largest carbon sink, and those in Boreal Asia,
805 Temperate Asia and Europe are also very strong and comparable. However, in CT2017,
806 the carbon sinks are mainly distributed in Boreal Asia and Temperate Asia, accounting
807 for more than 70% of the total sink in Northern Lands. The sinks in Temperate North
808 America and Europe are very weak or even neutral. In Tropical Lands, this study shows

删除了: 3

811 strong carbon sinks in Tropical South America and Tropical Asia, and a weak sink in
812 Africa, while CT2017 shows an opposite pattern. In Southern Lands, this study shows
813 comparable sinks in Temperate South America and Australia, while CT2017 shows a
814 strong sink in Temperate South America and very weak one in Australia. Compared
815 with JCS, except for Temperate North America and Southern Africa, the carbon sinks
816 are comparable in other regions. Constraining with different observations might be one
817 of the main reasons among these studies. Many studies have shown differences between
818 the constraints with in situ observations and XCO₂ retrievals (e.g., Wang et al., 2019;
819 Deng et al., 2014). Besides, these differences may be also related to the different prior
820 BIO carbon fluxes among these studies, especially for the tropical land. The distribution
821 of the posterior BIO fluxes in this study and CT2017 are consistent with the
822 corresponding prior fluxes in the tropical land (Table 4). Using the same GOSAT XCO₂
823 retrievals, Deng et al. (2014) adopted a similar prior flux with this study, which was
824 also simulated using the BEPS model but globally neutralized, to infer the land fluxes
825 of 2010, their distributions are roughly consistent with this study, while Wang et al.
826 (2019) applied the prior flux from CT2016 to optimizing the fluxes in 2015, and they
827 showed a similar distribution of land sinks over tropical lands to that of CT2017.

删除了: 3

828 **Table 4.** Regional BIO and FIRE flux in the 11 TRANSCOM land regions (PgC yr⁻¹)

删除了: 3

Regions	Fire	This Study		CT2017		JCS
		Prior	Posterior	Prior	Posterior	
Boreal North America	0.065	-0.26±0.82	-0.28±0.75	-0.05	-0.39	-0.31
Temperate North America	0.022	-0.49±1.62	-0.88±1.19	-0.14	-0.23	-0.21
Tropical South America	0.220	-0.66±1.28	-0.66±1.20	0.02	-0.11	-0.43
Temperate South America	0.142	-0.30±1.27	-0.15±0.93	-0.16	-0.42	0.13
Northern Africa	0.385	-0.18±1.50	-0.05±1.41	-0.47	-0.82	-0.11
Southern Africa	0.628	0.01±1.35	-0.14±1.14	-0.63	-0.55	-0.66
Boreal Asia	0.097	-0.61±1.24	-0.45±1.05	-0.18	-0.99	-0.51
Temperate Asia	0.065	-0.51±1.23	-0.42±1.10	-0.15	-0.66	-0.69
Tropical Asia	0.258	-0.45±0.77	-0.47±0.71	-0.05	-0.07	-0.73
Australia	0.097	-0.16±0.50	-0.23±0.45	-0.15	-0.07	-0.08
Europe	0.015	-0.46±1.31	-0.52±1.05	-0.18	0	-0.44
Northern Lands*	0.26	-2.33±2.91	-2.55±2.33	-0.7	-2.27	-2.16
Tropical Lands**	1.49	-1.28±2.57	-1.32±2.34	-1.13	-1.55	-1.93
Southern Lands***	0.24	-0.46±1.38	-0.38±1.04	-0.31	-0.49	0.05

831 *Northern lands include Boreal North America, Temperate North America, Boreal Asia, Temperate
832 Asia and Europe; **Tropical Lands include Tropical South America, Tropical Asia, Northern Africa
833 and Southern Africa; ***Southern Lands include Temperate South America and Australia.

834 Compared with other studies, the land fluxes (including FIRE but excluding
835 FOSSIL) in South America (-0.45 ± 1.51 PgC yr⁻¹), Europe (-0.51 ± 1.05 PgC yr⁻¹),
836 Boreal Asia (-0.35 ± 1.05 PgC yr⁻¹), Temperate Asia (-0.35 ± 1.10 PgC yr⁻¹), Tropical Asia
837 (-0.21 ± 0.71 PgC yr⁻¹), and Australia (-0.13 ± 0.45 PgC yr⁻¹) are comparable with the
838 forest sinks in these regions during 2000-2007 estimated using forest inventory data by
839 Pan et al. (2011). However, the land fluxes in Africa and North America are
840 significantly different from the estimates of Pan et al. (2011). In North America, based
841 on inventory-based calculations, the Second State of the Carbon Cycle Report
842 (SOCCR2, Hayes et al., 2018) estimated that the average annual net land ecosystem
843 flux was -0.96 PgC yr⁻¹, and after considering the outgassing and wood products
844 emissions, they reported the land-based carbon sink was -0.606 PgC yr⁻¹ ($\pm 75\%$) during
845 the 2004 to 2013 time period. The land flux estimated in this study (-1.07 PgC yr⁻¹) is
846 close to the bottom-up estimate of the net land ecosystem flux, but much stronger than
847 the reported land-based carbon sink of SOCCR2. In Africa, Ciais et al. (2011) shown a
848 comprehensive estimate for its carbon balance, given a sink of -0.2 PgC yr⁻¹ (excluding
849 land-use change emissions) based upon observations. Our estimate of the BIO flux in
850 Africa is very consistent with this result. Moreover, most recently, Palmer et al. (2019)
851 inferred the carbon fluxes of pan-tropical lands in 2015 and 2016 using both GOSAT
852 and the NASA Orbiting Carbon Observatory (OCO-2) XCO₂ retrievals, and their
853 estimated net carbon emissions from African biosphere dominate pan-tropical
854 atmospheric CO₂ signals are similar to the results of this study. In Boreal Asia, the land
855 sink estimated by bottom-up approaches was in the range of $-0.11 \sim -0.76$ PgC yr⁻¹
856 (Hayes et al., 2011; Nilsson et al., 2003; Dolman et al., 2012; Zamolodchikov et al.,
857 2017). CT usually reports a very strong carbon sink (Jacobson et al. 2020; Peter et al.,
858 2007; Zhang et al., 2014), one possible reason is that there are no enough surface
859 observations in Asia boreal regions. Saeki et al. (2013b) conducted an inversion with a
860 focus on the Siberia region, and also derived a large sink of -0.56 ± 0.79 PgC yr⁻¹ only

删除了: arbon

删除了: racker

删除了: er

864 using the NOAA data, but after adding additional observations in Siberia, they obtained
865 a weaker uptake of -0.35 ± 0.61 PgC yr⁻¹. Our estimate (-0.35 ± 1.05 PgC yr⁻¹) is in the
866 range of bottom-up estimates, and very consistent with the Siberia-focused inversion
867 (Saeki et al., 2013b). In Europe, previous GOSAT-based inversions consistently derived
868 a very large European sink, which was in the range of $-0.6 \sim -1.8$ PgC yr⁻¹ (Basu et al.,
869 2013, Chevallier et al., 2014; Deng et al., 2014), while the ones constrained using
870 surface observations were much weaker, in the range of $0 \sim -0.4$ PgC yr⁻¹ (Peters et al.,
871 2007, 2010; Peylin et al., 2013; Scholze et al., 2019). Our estimate of the BIO flux in
872 Europe is smaller than the previous GOSAT-based inversions, and close to the estimate
873 of Pelylin et al. (2013). In the Amazon region, the posterior land flux is -0.45 ± 1.28 PgC
874 yr⁻¹, which is in the range of the previous long-term forest biomass sink estimates of $-$
875 $0.28 \sim -0.49$ PgC yr⁻¹ (Phillips et al., 2009; Brienen et al., 2015), but larger than the
876 other inversions (e.g., Deng et al., 2016; Gatti et al., 2014).

877 **4.5 Interannual variations**

878 **4.5.1 Global land and ocean fluxes**

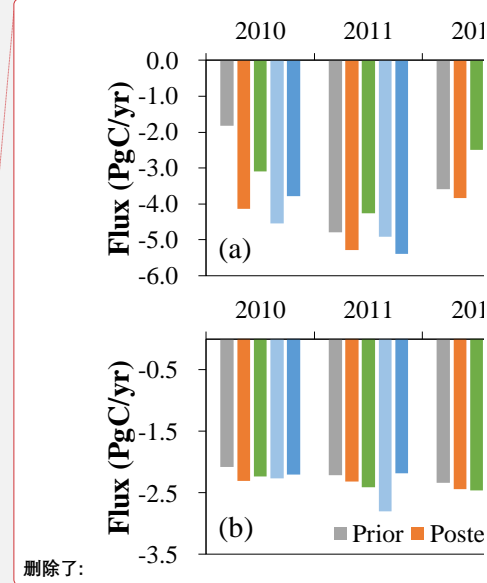
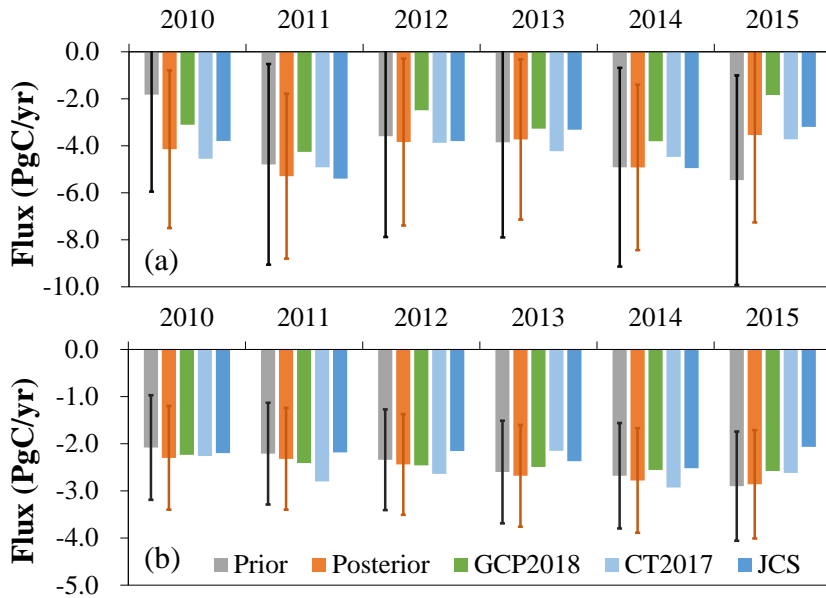
879 Figure 8 shows the interannual variations of the prior and posterior BIO and OCN
880 fluxes. Overall, from 2010 to 2015, the prior BIO fluxes show an increasing trend, but
881 for the posterior fluxes, there is no significant trend. Large differences between the prior
882 and the posterior fluxes mainly occur in 2010 and 2015. In 2010, the posterior sink is
883 much stronger than the prior, while in 2015, the posterior sink is much weaker than the
884 prior. For the OCN flux, both prior and posterior fluxes show consistently upward
885 trends, and except for 2015, the posterior sinks are basically stronger than the prior ones
886 every year. For the AGR (Figure 9), the prior sink shows a significant downward trend,
887 while the posterior one shows a slightly increasing trend. The same as the BIO fluxes,
888 large differences mainly occur in 2010 and 2015.

删除了: 4

删除了: 4

删除了: 7

删除了: 8



893

894 **Figure 8.** Interannual variations of global (a) BIO and (b) OCN fluxes of the prior and
 895 posterior as well as GCP2018, CarbonTracker 2017 (CT2017) and Jena CarboScope
 896 (JCS)

897 Compared with the other products, the interannual variations of the posterior BIO
 898 fluxes (Figure 8a) are consistent with the inversions of CT2017 and JCS, and the
 899 estimates of GCP2018. For each year, the inversions of this study are all in the range of
 900 CT2017 and JCS, but higher than GCP2018. However, because GCP2018 has the item
 901 of budget imbalance and the land-use change emission is different from the FIRE
 902 emission, the BIO flux in GCP2018 is different from this study, so direct comparison
 903 with GCP2018 is not meaningful. For OCN fluxes, overall, there are no significant
 904 differences among different estimates, and the upward trend of this study is similar to
 905 that of GCP2018, and higher than those of CT2017 and JCS. The interannual variation
 906 of AGR in this study is also very consistent with GCP2018 (Figure 9). Except for 2012
 907 and 2015, the absolute deviations of AGR between this study and GCP2018 are within
 908 0.3 PgC yr⁻¹.

删除了: 7

删除了: 7a

删除了: 8

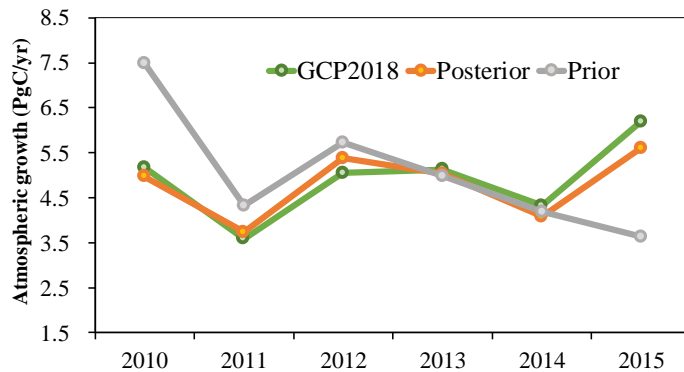


Figure 9. Interannual variations of the atmospheric CO₂ growth rates

删除了: 8

4.5.2 Regional land fluxes

删除了: 4

Figure 10a, b, and c show the prior and posterior interannual variations of the BIO fluxes in Northern Lands, Tropical Lands and Southern Lands, respectively. In Northern Lands, the interannual variations of both prior and posterior fluxes are similar to the corresponding global land totals (Figure 8a), i.e., upward trend for the prior flux and no trend with the posterior one, indicating that the interannual variations of global BIO fluxes are dominated by the fluxes in Northern Lands. In Tropical Lands, the interannual variations of posterior fluxes are similar to the prior ones, however, compared with the prior sinks in 2010 and 2011, the posterior sinks are much stronger, while in 2013 and 2015, they are much weaker. In Southern Lands, there are large differences for the interannual variations between the prior and posterior fluxes. For the prior flux, the highest sink is in 2011 and the weakest in 2012, and after that, it increases year by year, while for the posterior flux, the sink decreases from 2010 to 2013, and then increases.

删除了: 9

删除了: 7a

913

914

915

916

917

918

919

920

921

922

923

924

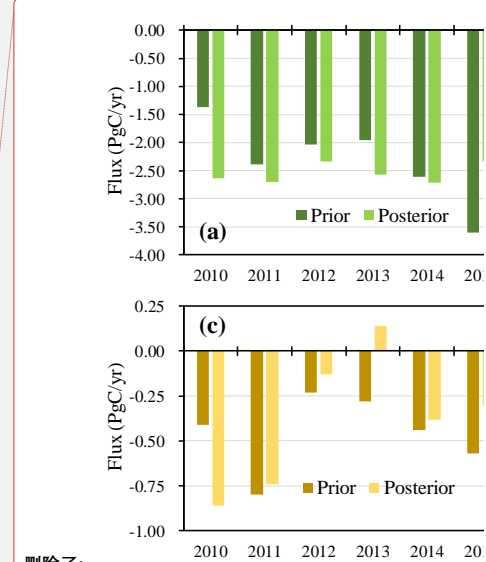
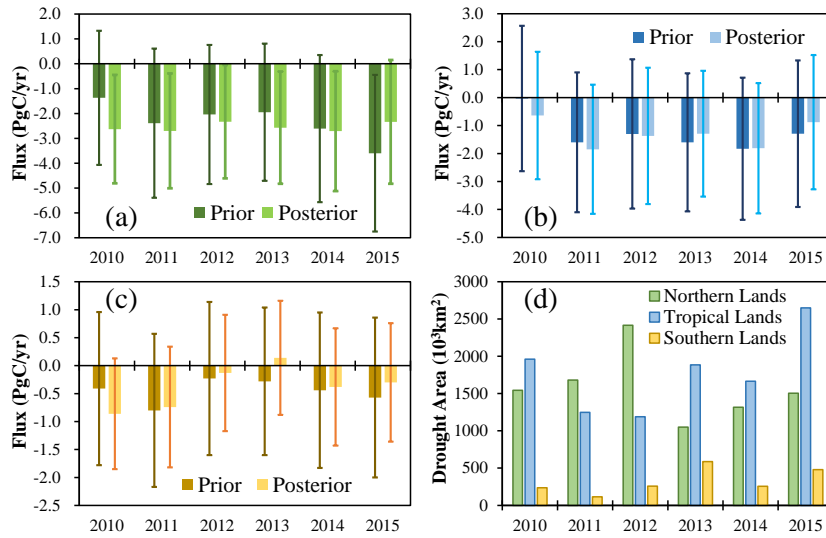
925

926

927

928

929



删除了:

删除了: 9

删除了: 9

Figure 10. Prior and posterior interannual variations of the BIO fluxes in (a) Northern Lands, (b) Tropical Lands, and (c) Southern Lands, respectively, and (d) severe drought areas of above 3 regions.

Drought is one of the most important factors that affect terrestrial carbon sinks, and generally, severe drought will significantly reduce carbon sinks (e.g., Ma et al., 2012; Zhao and Running, 2010; Ciais et al., 2005; Gatti et al., 2014; Phillips et al., 2009; Vicente-Serrano et al., 2013). Previous studies (e.g., Liu et al., 2018) have used the GOSAT XCO₂ retrievals to infer the impact of droughts on terrestrial ecosystem carbon uptake anomalies. Figure 10d shows the severe drought areas (SDAs) in the 3 large regions every year, which were calculated according to the monthly Standardised Precipitation-Evapotranspiration Index at 12-month time scales (SPEI12) (Beguería et al., 2010). Here, the database of SPEIbase v2.5 is used, and the severe drought is defined as SPEI12 less than -1.5 (Paulo et al., 2012). In addition, only the severe drought that happens in forests, shrubs and crops are counted in this study. It could be found that the posterior fluxes have better correlations with the SDAs in all 3 regions, i.e. a larger SDA leads to a weaker carbon sink, and vice versa. The correlation coefficients between carbon sinks and SDAs in Northern Lands, Tropical Lands and

955 Southern Lands increase from prior values of -0.1, -0.25 and -0.44 to -0.53, -0.67 and -
956 0.76, respectively, indicating that the inversion has improved the interannual variations
957 of BIO fluxes in large scales. In addition, strong El Niño event happened during
958 2015~2016, and many researches have studied the responses of tropical land carbon
959 fluxes to this strong El Niño event (e.g., Wang et al., 2018b; Liu et al., 2017; Bastos et
960 al., 2018; Koren et al., 2018). Liu et al. (2017) found that relative to the 2011 La Niña,
961 the pantropical biosphere released 2.5 ± 0.34 PgC more carbon into the atmosphere in
962 2015. Bastos et al. (2018) showed a smaller difference of carbon fluxes between 2015
963 and 2011 using both bottom-up and top-down approaches, which was in the range of
964 $-0.7 \sim -1.9$ PgC yr⁻¹. In this study, compared with the prior, our inversion significantly
965 enhances the difference between 2011 and 2015 (Figure 10b), and shows that 2015
966 released 1.35 PgC more than 2011 in the pantropical region (defined as Liu et al., 2017),
967 which is much smaller than Liu et al.'s result, but agree well with the result of Bastos
968 et al. (2018).

删除了: 9

969 Moreover, Figure 11 shows the prior and posterior interannual variations of the
970 BIO fluxes on the 11 TRANSCOM land regions. In North America, including
971 Temperate North America and Boreal North America, the prior fluxes show an upward
972 trend, while the posterior fluxes show a downward trend. In Boreal Asia and Temperate
973 Asia, there are significant upward trends for the prior fluxes, but no significant trends
974 are found in the posterior fluxes. In Temperate South America, although the prior and
975 posterior fluxes show trends of weakening first and then increasing, the years in which
976 the carbon sink is weakest are not consistent: the prior flux is weakest in 2012, while
977 the posterior one is in 2013. Similarly, in northern Africa, the prior and posterior fluxes
978 show a trend of increasing and then decreasing, but the prior flux is the largest in 2014,
979 while the posterior one is strongest in 2011. In other regions, i.e., Tropical South
980 America, Tropical Asia, Southern Africa, Australia and Europe, the trends between the
981 prior and posterior fluxes are similar, especially in Tropical South America and Tropical
982 Asia, the prior and posterior fluxes are very close every year. Among them, in Southern
983 Africa and Australia, the posterior fluxes have more significant interannual variations

删除了: 10

986 than the prior fluxes, and in Europe, the posterior sink is much weaker in 2015, and
987 stronger in 2010 and 2013 than the prior one.

988 The same as above, we also investigate the relationships between the interannual
989 variations of carbon sinks and SDAs in the 11 TRANSCOM land regions. As shown in
990 Table 5, in Temperate South America, Boreal Asia, and Europe, the posterior sinks have
991 a better correlation with the SDAs than the prior sinks, especially in Europe, the
992 correlation coefficient increases from a prior value of -0.33 to -0.85. However, in other
993 regions, there is no obvious improvement, and in some regions, the relationships are
994 even getting worse, such as Boreal North America, Temperate North America, Northern
995 Africa and Southern Africa. One possible reason is that there are usually higher annual
996 mean temperatures in drought years, which might extend the growing season of
997 vegetation, thereby enhance the carbon uptake and offset the impacts of drought. A
998 previous study (Wolf et al., 2016) showed that in 2012, Temperate North America
999 experienced an extreme summer drought event, and along with the warmest spring on
1000 record. They quantified the impact of this climate anomaly on the carbon cycle and
1001 concluded that the warm spring largely increased spring carbon uptake, and thus
1002 compensated for reduced carbon uptake induced by the summer drought. Liu et al.
1003 (2018) reported that because of the compensating effect of the carbon flux anomalies
1004 between northern and southern US in 2011 and between spring and summer in 2012,
1005 the annual carbon uptake decreased by 0.10 ± 0.16 PgC in 2011, and increased by
1006 0.10 ± 0.16 GtC in 2012 over US compared with the averaged state. In this study,
1007 compared with the mean flux during 2010-2015, the carbon sink in Temperate North
1008 America decreased by 0.09 PgC yr⁻¹ in 2011, and increased by 0.14 PgC yr⁻¹ in 2012,
1009 which is very close to the result of Liu et al. (2018). In Australia, both the prior and
1010 posterior fluxes have very good relationships with the SDAs. The significantly
1011 enhanced carbon uptake during 2010-2012 is consistent with the finding in Detmers et
1012 al. (2015), who inferred an even stronger carbon sink of -0.77 ± 0.10 PgC yr⁻¹ from the
1013 end of 2010 to early 2012 using the GOSAT XCO₂ product, and they confirmed that
1014 this enhanced sink is related to the strong La Niña episode, which brought a record-

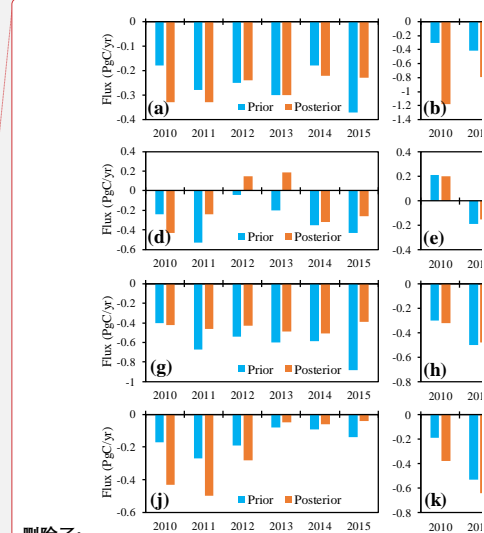
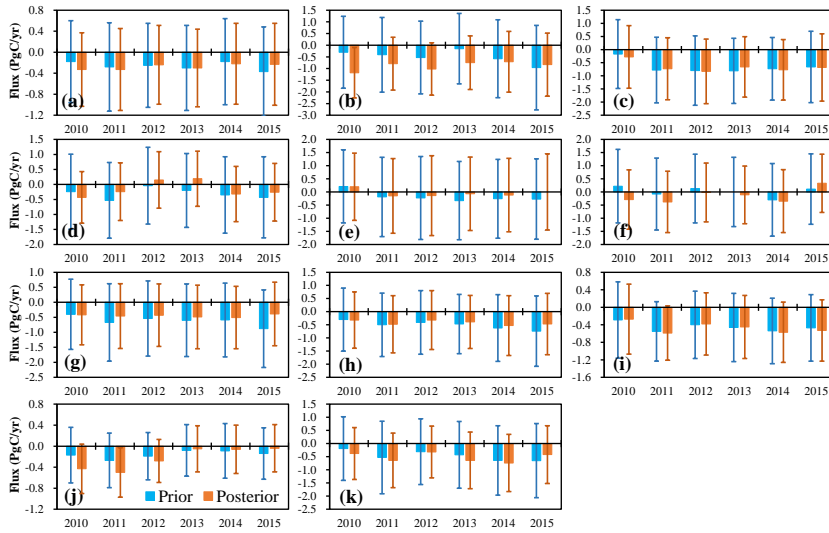
删除了: 4

1016 breaking amount of precipitation, resulting in an enhanced growth of vegetation. In
1017 Tropical South America, the impacts of the 2010 drought on the carbon uptake over
1018 Amazon have been extensively studied (e.g., Doughty et al., 2015; Gatti et al., 2014;
1019 van der Laan-Luijkx et al., 2015). 2010 is a drought year, while 2011 is a wet year in
1020 the Amazon region, compared to 2011, Gatti et al. (2014) estimated the no-fire carbon
1021 exchange was reduced by 0.22 PgC yr⁻¹, van der Laan-Luijkx et al. (2015) derived a
1022 decrease of biospheric uptake ranging from 0.08 to 0.26 PgC yr⁻¹, and Doughty et al.
1023 (2015) concluded that drought suppressed Amazon-wide photosynthesis by 0.23–0.53
1024 PgC yr⁻¹. In this study, our inversion reduces the difference of carbon uptake between
1025 2010 and 2011 from a prior of 0.62 PgC yr⁻¹ to 0.28 PgC yr⁻¹, which is much more
1026 consistent with the previous estimates.

1027 Carbon uptake occurs mainly through photosynthesis of vegetation leaves. Leaf
1028 area index (LAI) is a measure of leaf area per unit area. Buchmann and Schulze (1999)
1029 shown that there are strong relationships between the interannual changes of carbon
1030 uptake and LAI in grasslands, C4 crops, and coniferous forests, but no significant
1031 relationship in broad-leaved forests; Chen et al. (2019) also showed that from 1981 to
1032 2016, the increase in LAI contributed significantly to the increase in global BIO carbon
1033 sinks. Therefore, we further investigate the relationships between the interannual
1034 changes of carbon sinks and LAIs in the 11 TRANSCOM regions (Table 5). Here, the
1035 LAI data are from the GIMMS LAI3g product, which has a spatial resolution of 1/12
1036 degree and a time interval of 15 days (Zhu et al., 2013). As shown in Table 5, in Boreal
1037 North America, Temperate North America, Northern Africa and Southern Africa,
1038 compared with the prior fluxes, there are better relationships between the posterior
1039 carbon sinks and LAIs, the correlation coefficients increase from prior values of -0.4,
1040 0.31 and 0.35 to 0.62, 0.73 and 0.90 respectively, suggesting that the inversion of this
1041 study may also improve the interannual variations of carbon sinks in these 4 regions at
1042 a certain extent.

删除了: 4

删除了: 4



删除了:

删除了: 10

删除了: 4

Figure 11. Prior and posterior interannual variations of the BIO fluxes on (a) Boreal North America, (b) Temperate North America, (c) Tropical South America, (d) Temperate South America, (e) Northern Africa, (f) Southern Africa, (g) Boreal Asia, (h) Temperate Asia, (i) Tropical Asia, (j) Australia, and (k) Europe

Table 5. Correlation coefficients of severe drought areas (SDAs) and regional mean LAI with the BIO sinks in each region

Regions	SDA		LAI	
	Prior	Posterior	Prior	Posterior
Boreal North America	-0.29	0.36	-0.4	0.62
Temperate North America	-0.54	-0.27	0.31	0.73
Tropical South America	-0.1	-0.2	0.64	0.49
Temperate South America	-0.41	-0.74	0.72	0.24
Northern Africa	0.51	0.2	0.81	0.89
Southern Africa	-0.53	0.41	0.35	0.9
Boreal Asia	-0.17	-0.35	0.49	0.1
Temperate Asia	0.33	0.33	0.55	0.38
Tropical Asia	-0.03	0.16	0.69	0.71
Australia	-0.85	-0.73	0.88	0.83
Europe	-0.33	-0.85	0.85	0.58

1045

1046

1047

1048

1049

1050

1051

1052

1053

1054

1058 **5. Summary and Conclusions**

1059 In this study, we upgrade the GCAS system to GCASv2 with new assimilation
1060 algorithms, procedures and a localization scheme, a higher assimilation parameter
1061 resolution, and the ability to assimilate XCO₂ retrievals. Then, we use the GOSAT
1062 XCO₂ retrievals to constrain terrestrial ecosystem and ocean carbon fluxes from May
1063 1, 2009 to Dec 31, 2015, using the GCASv2 system. We compare the simulated prior
1064 and posterior XCO₂ against the corresponding GOSAT XCO₂ retrievals to test the
1065 effectiveness of the assimilation system and evaluate the posterior carbon fluxes by
1066 comparing the posterior CO₂ mixing ratios against observations from 52 surface flask
1067 sites. The distribution and interannual variations of the posterior carbon fluxes at both
1068 global and regional scales from 2010 to 2015 are shown and discussed.

1069 Compared with the GOSAT XCO₂ retrievals, the global mean BIAS and RMSE
1070 decrease from prior values of 1.8±1.3 and 2.2 ppm to -0.0±1.1 and 1.1 ppm, respectively,
1071 indicating that the GCASv2 system works well with the GOSAT XCO₂ retrievals.
1072 Independent evaluations using surface flask CO₂ concentrations showed that the
1073 posterior carbon fluxes could significantly improve the modeling of atmospheric CO₂
1074 concentrations, with the global mean BIAS and RMSE decreasing from prior values of
1075 1.6±1.8 and 2.4 ppm to -0.5±1.8 and 1.9 ppm, respectively. The large negative biases
1076 are mainly distributed in North America, Europe, indicating the overestimates of carbon
1077 sinks over these areas. Evaluations also show that the biases gradually increase along
1078 with the time in most tropical and southern hemisphere ocean sites, but no accumulation
1079 is found at most land sites, indicating that globally, the carbon sinks may be
1080 overestimated every year, but in different lands, the deviations of the estimates may
1081 differ each year.

1082 Globally, the mean annual BIO carbon sink and the interannual variations
1083 inferred in this study are very close to the estimates of CT2017 during the study period,
1084 and the estimated mean AGR and interannual changes are also very close to the
1085 observations, with mean annual bias of -0.11 PgC yr⁻¹. Regionally, the inversion shows

1086 that in the northern lands, the carbon sink of Temperate North America is the strongest,
1087 and those in Boreal Asia, Temperate Asia and Europe are also very strong and
1088 comparable; in the tropics, there are strong sinks in Tropical South America and
1089 Tropical Asia, but a very weak sink in Africa. These distributions are significantly
1090 different from the estimates of CT2017, probably due to the different prior fluxes and
1091 CO₂ observations used for inversion. However, our estimates in most regions or
1092 continents are comparable or in the range of previous bottom-up estimates. The
1093 inversion also changed the interannual variations of carbon sinks in most TRANSCOM
1094 and hemisphere scale land regions, leading to their better relationship with the
1095 variations of severe drought or LAI, indicating that the inversion with GOSAT XCO₂
1096 retrievals may help to better understand the interannual variations of regional carbon
1097 fluxes.

1098

1099 **Data availability**

1100 The code of GCASv2 system and the inversion results of this study are available to the
1101 community and can be accessed upon request from Fei Jiang (jiangf@nju.edu.cn) at
1102 Nanjing University.

1103 **Author contributions**

1104 FJ, JC and WJ designed the research; FJ run the model, analyzed the results and wrote
1105 the paper; HW handled the GOSAT XCO₂ retrievals; WH analyzed the drought data;
1106 XL run the BEPS model; FJ lead the update of the GCAS system, and XT, HW, JW, SF,
1107 GL, ZC, SZ, JL, WH, and MW participated in it; RL, PS and PK provided the surface
1108 CO₂ observations; JC, WJ and HW participated in the discussion of the inversion results
1109 and provided input on the paper for revision before submission.

1110 **Competing interests**

1111 The authors declare that they have no conflict of interest.

1112 **Acknowledgements**

1113 This work is supported by the National Key R&D Program of China (Grant No:
1114 2016YFA0600204). We acknowledge all atmospheric data providers to
1115 obspack_co2_1_GLOBALVIEWplus_v5.0_2019_08_12. We especially thank Pieter
1116 Tans, Ed Dlugokencky, Kenneth Schuldt at NOAA ESRL, USA and Ray Langenfelds,
1117 Paul Steele, Paul Krummel at CSIRO, Australia for their great efforts on CO₂
1118 observations and data distributions. CarbonTracker CT2017 results are provided by
1119 NOAA ESRL, Boulder, Colorado, USA, from the website at
1120 <http://carbontracker.noaa.gov>. The GOSAT data are produced by the OCO project at the
1121 Jet Propulsion Laboratory, California Institute of Technology, and obtained from the
1122 data archive at the NASA Goddard Earth Science Data and Information Services Center.
1123 We are also grateful to the High-Performance Computing Center (HPCC) of Nanjing
1124 University for doing the numerical calculations in this paper on its blade cluster system.
1125

1126 **Reference**

- 1127 Andres, R. J., Gregg, J. S., Losey, L., Marland, G. and Boden, T. A.: Monthly, global emissions
1128 of carbon dioxide from fossil fuel consumption. *Tellus B*, 63(3), 309–327,
1129 <https://doi.org/10.1111/j.1600-0889.2011.00530.x>, 2011.
- 1130 Archer, C. L., and Jacobson, M. Z.: Evaluation of global wind power, *J. Geophys. Res.*, 110,
1131 D12110, <https://doi.org/10.1029/2004JD005462>, 2005.
- 1132 Bastos, A., Friedlingstein, P., Sitch, S., Chen, C., Mialon, A., Wigneron, J.-P., Arora, V. K.,
1133 Briggs, P. R., Canadell, J. G., and Ciais, P.: Impact of the 2015/2016 El Niño on the
1134 terrestrial carbon cycle constrained by bottom-up and top-down approaches. *Philosophical
1135 Transactions of the Royal Society B: Biological Sciences*, 373(1760), 20170304,
1136 <https://doi.org/10.1098/rstb.2017.0304>, 2018.
- 1137 Basu, S., Guerlet, S., Butz, A., Houweling, S., Hasekamp, O., Aben, I., Krummel, P., Steele, P.,
1138 Langenfelds, R., Torn, M., Biraud, S., Stephens, B., Andrews, A., and Worthy, D.: Global
1139 CO₂ fluxes estimated from GOSAT retrievals of total column CO₂, *Atmos. Chem. Phys.*, 13,
1140 8695–8717, <https://doi.org/10.5194/acp-13-8695-2013>, 2013.
- 1141 Beguería, S., Vicente-Serrano, S. M., and Angulo-Martinez, M.: A Multiscalar Global Drought
1142 Dataset: The SPEIbase: A New Gridded Product for the Analysis of Drought Variability and
1143 Impacts. *Bulletin of The American Meteorological Society - BULL AMER METEOROL
1144 SOC*, 91, <https://doi.org/10.1175/2010BAMS2988.1>, 2010.

- 1145 Brienen, R. J. W., Phillips, O. L., Feldpausch, T. R., Gloor, E., Baker, T. R., Lloyd, J., Lopez-
1146 Gonzalez, G., Monteagudo-Mendoza, A., Malhi, Y., Lewis, S. L., Martinez, R. V., Alexiades,
1147 M., Davila, E. A., Alvarez-Loayza, P., Andrade, A., Aragao, L., Araujo-Murakami, A., Arets,
1148 E., Arroyo, L., Aymard, G. A., Banki, O. S., Baraloto, C., Barroso, J., Bonal, D., Boot, R.
1149 G. A., Camargo, J. L. C., Castilho, C. V., Chama, V., Chao, K. J., Chave, J., Comiskey, J.
1150 A., Valverde, F. C., da Costa, L., de Oliveira, E. A., Di Fiore, A., Erwin, T. L., Fauset, S.,
1151 Forsthofer, M., Galbraith, D. R., Grahame, E. S., Groot, N., Hérault, B., Higuchi, N.,
1152 Coronado, E. N. H., Keeling, H., Killeen, T. J., Laurance, W. F., Laurance, S., Licona, J.,
1153 Magnussen, W. E., Marimon, B. S., Marimon, B. H., Mendoza, C., Neill, D. A., Nogueira,
1154 E. M., Nunez, P., Camacho, N. C. P., Parada, A., Pardo-Molina, G., Peacock, J., Pena-Claros,
1155 M., Pickavance, G. C., Pitman, N. C. A., Poorter, L., Prieto, A., Quesada, C. A., Ramirez,
1156 F., Ramirez-Angulo, H., Restrepo, Z., Roopsind, A., Rudas, A., Salomao, R. P., Schwarz,
1157 M., Silva, N., Silva-Espejo, J. E., Silveira, M., Stropp, J., Talbot, J., ter Steege, H., Teran-
1158 Aguilar, J., Terborgh, J., Thomas-Caesar, R., Toledo, M., Torello-Raventos, M., Umetsu, R.
1159 K., Van der Heijden, G. M. F., Van der Hout, P., Vieira, I. C. G., Vieira, S. A., Vilanova, E.,
1160 Vos, V. A., and Zagt, R. J.: Long-term decline of the Amazon carbon sink. *Nature*, 519, 344–
1161 348, <https://doi.org/10.1038/nature14283>, 2015.
- 1162 [Bruhwiler, L. M. P., Michalak, A. M., Peters, W., Baker, D. F., and Tans, P.: An improved](#)
1163 [Kalman Smoother for atmospheric inversions, *Atmos. Chem. Phys.*, 5, 2691–2702,](#)
1164 <https://doi.org/10.5194/acp-5-2691-2005>, 2005.
- 1165 Buchmann, N., and Schulze, E.D.: Net CO₂ and H₂O fluxes of terrestrial ecosystems, *Global*
1166 *Biogeochem. Cycles*, 13(3), 751–760, <https://doi.org/10.1029/1999GB900016>, 1999.
- 1167 Buitenhuis, E., Le Quéré, C., Aumont, O., Beaugrand, G., Bunker, A., Hirst, A., Ikeda, T.,
1168 O'Brien, T., Piontkovski, S., and Straille, D.: Biogeochemical fluxes through
1169 mesozooplankton, *Global Biogeochem. Cycles*, 20, GB2003,
1170 <https://doi.org/10.1029/2005GB002511>, 2006.
- 1171 Botta, A., Ramankutty, N., and Foley, J. A.: LBA-ECO LC-04 IBIS model simulations for the
1172 Amazon and Tocantins Basins: 1921–1998, ORNL DAAC, Oak Ridge, Tennessee, USA,
1173 <https://doi.org/10.3334/ORNLDAAC/1139>, 2012.
- 1174 [Bousquet, P., Peylin, P., Ciais, P., Le Quéré, C., Friedlingstein, P., and Tans, P. P.: Regional](#)
1175 [Changes in Carbon Dioxide Fluxes of Land and Oceans Since 1980, 290 \(5495\), 1342–1346,](#)
1176 <https://doi.org/10.1126/science.290.5495.1342>, 2000.
- 1177 [Byrne, B., Jones, D. B. A., Strong, K., Polavarapu, S. M., Harper, A. B., Baker, D. F., and](#)
1178 [Maksyutov, S.: On what scales can GOSAT flux inversions constrain anomalies in terrestrial](#)
1179 [ecosystems?, *Atmos. Chem. Phys.*, 19, 13017–13035, \[https://doi.org/10.5194/acp-19-\]\(https://doi.org/10.5194/acp-19-13017-2019\)](#)
1180 [13017-2019](#), 2019.
- 1181 Chen, J. M., Ju, W., Ciais, P., Viovy, N., Liu, R. G., Liu, Y., and Lu, X. H.: Vegetation structural
1182 change since 1981 significantly enhanced the terrestrial carbon sink. *Nat. Commun.*, 10,
1183 4259, <https://doi.org/10.1038/s41467-019-12257-8>, 2019.
- 1184 Chen, J. M., Ju, W., Cihlar, J., Price, D., Liu, J., Chen, W., Pan, J., Black, A. and Barr, A.: Spatial

- 1185 distribution of carbon sources and sinks in Canada's forests. *Tellus B*, 55, 622–642,
1186 <https://doi.org/10.1034/j.1600-0889.2003.00036.x>, 2003.
- 1187 Chen, J. M., Liu, J., Cihlar, J., and Goulden, M. L.: Daily canopy photosynthesis model through
1188 temporal and spatial scaling for remote sensing applications, *Ecol. Modell.*, 124, 99–119,
1189 [https://doi.org/10.1016/S0304-3800\(99\)00156-8](https://doi.org/10.1016/S0304-3800(99)00156-8), 1999.
- 1190 Chen, J. M., Menges, C.H., and Leblanc, S.G.: Global mapping of foliage clumping index using
1191 multi-angular satellite data, *Remote Sens. Environ.*, 97 (4), 447–457,
1192 <https://doi.org/10.1016/j.rse.2005.05.003>, 2005.
- 1193 Chevallier, F., Breon, F.-M., and Rayner, P. J.: Contribution of the Orbiting Carbon Observatory
1194 to the estimation of CO₂ sources and sinks: Theoretical study in a variational data
1195 assimilation framework, *J. Geophys. Res.-Atmos.*, 112, d09307,
1196 <https://doi.org/10.1029/2006JD007375>, 2007.
- 1197 Chevallier, F., Palmer, P. I., Feng, L., Boesch, H., O'Dell, C. W., and Bousquet, P.: Toward
1198 robust and consistent regional CO₂ flux estimates from in situ and spaceborne
1199 measurements of atmospheric CO₂, *Geophys. Res. Lett.*, 41, 1065–1070,
1200 <https://doi.org/10.1002/2013GL058772>, 2014.
- 1201 [Chevallier, F., Remaud, M., O'Dell, C. W., Baker, D., Peylin, P., and Cozic, A.: Objective](#)
1202 [evaluation of surface- and satellite-driven carbon dioxide atmospheric inversions, *Atmos.*](#)
1203 [*Chem. Phys.*, 19, 14233–14251, <https://doi.org/10.5194/acp-19-14233-2019>, 2019.](#)
- 1204 Ciais, P., Reichstein, M., Viovy, N., Granier, A., Ogee, J., Allard, V., Aubinet, M., Buchmann,
1205 N., Bernhofer, C., Carrara, A., Chevallier, F., De Noblet, N., Friend, A. D., Friedlingstein,
1206 P., Grunwald, T., Heinesch, B., Keronen, P., Knohl, A., Krinner, G., Loustau, D., Manca, G.,
1207 Matteucci, G., Miglietta, F., Ourcival, J. M., Papale, D., Pilegaard, K., Rambal, S., Seufert,
1208 G., Soussana, J. F., Sanz, M. J., Schulze, E. D., Vesala, T., and Valentini, R.: Europewide
1209 reduction in primary productivity caused by the heat and drought in 2003, *Nature*, 437, 529–
1210 533, <https://doi.org/10.1038/nature03972>, 2005.
- 1211 Ciais, P., Bombelli, A., Williams, M., Piao, S.L., Chave, J., Ryan, C.M., Henry, M., Brender, P.,
1212 and Valentini, R.: The carbon balance of Africa: synthesis of recent research studies, *Phil.*
1213 *Trans. Roy. Soc. Lond. Math. Phys. Eng. Sci.*, 369, 2038–2057,
1214 <https://doi.org/10.1098/rsta.2010.0328>, 2011.
- 1215 [Connor, B. J., Boesch, H., Toon, G., Sen, B., Miller, C., and Crisp, D.: Orbiting Carbon](#)
1216 [Observatory: Inverse method and prospective error analysis, *J. Geophys. Res.*, 113, D05305,](#)
1217 [\[doi:10.1029/2006JD008336\]\(https://doi.org/10.1029/2006JD008336\), 2008.](#)
- 1218 Crisp, D., Fisher, B., O'Dell, C., Frankenberg, C., Basilio, R., Bosch, H., Brown, L. R., Castano,
1219 R., Connor, B., Deutscher, N. M., Eldering, A., Griffith, D., Gunson, M., Kuze, A.,
1220 Mandrake, L., McDuffie, J., Messerschmidt, J., Miller, C. E., Morino, I., Natraj, V., Notholt,
1221 J., O'Brien, D. M., Oyafuso, F., Polonsky, I., Robinson, J., Salawitch, R., Sherlock, V.,
1222 Smyth, M., Suto, H., Taylor, T. E., Thompson, D. R., Wennberg, P. O., Wunch, D., and Yung,
1223 Y. L.: The ACOS CO₂ retrieval algorithm - Part II: Global XCO₂ data characterization.
1224 *Atmospheric Measurement Techniques*, 5 (4), 687–707, <https://doi.org/10.5194/amt-5-687->

- 1225 2012, 2012.
- 1226 Deng, F., Jones, D. B. A., Henze, D. K., Bousserez, N., Bowman, K. W., Fisher, J. B., Nassar,
1227 R., O'Dell, C., Wunch, D., Wennberg, P. O., Kort, E. A., Wofsy, S. C., Blumenstock, T.,
1228 Deutscher, N. M., Griffith, D. W. T., Hase, F., Heikkinen, P., Sherlock, V., Strong, K.,
1229 Sussmann, R., and Warneke, T.: Inferring regional sources and sinks of atmospheric CO₂
1230 from GOSAT XCO₂ data, *Atmos. Chem. Phys.*, 14, 3703–3727, [https://doi.org/10.5194/acp-](https://doi.org/10.5194/acp-14-3703-2014)
1231 14-3703-2014, 2014.
- 1232 Deng, F., Jones, D. B. A., O'Dell, C. W., Nassar, R., and Parazoo, N. C.: Combining GOSAT
1233 XCO₂ observations over land and ocean to improve regional CO₂ flux estimates, *J. Geophys.*
1234 *Res. Atmos.*, 121, 1896–1913, <https://doi.org/10.1002/2015JD024157>, 2016.
- 1235 Detmers, R. G., Hasekamp, O., Aben, I., Houweling, S., van Leeuwen, T. T., Butz, A., Landgraf,
1236 J., Köhler, P., Guanter, L., and Poulter, B.: Anomalous carbon uptake in Australia as seen
1237 by GOSAT, *Geophys. Res. Lett.*, 42, 8177–8184, <https://doi.org/10.1002/2015GL065161>,
1238 2015.
- 1239 Dlugokencky, E., and Tans, P.: Trends in atmospheric carbon dioxide, National Oceanic &
1240 Atmospheric Administration, Earth System Research Laboratory (NOAA/ESRL), available
1241 at <http://www.esrl.noaa.gov/gmd/ccgg/trends/global.html>, 2018.
- 1242 Doughty, C. E., Metcalfe, D. B., Girardin, C. A. J., Amezquita, F. F., Cabrera, D. G., Huasco,
1243 W. H., Silva-Espejo, J. E., Araujo-Murakami, A., da Costa, M. C., Rocha, W., Feldpausch,
1244 T. R., Mendoza, A. L. M., da Costa, A. C. L., Meir, P., Phillips, O. L., and Malhi, Y.: Drought
1245 impact on forest carbon dynamics and fluxes in Amazonia, *Nature*, 519, 78–82,
1246 <https://doi.org/10.1038/nature14213>, 2015.
- 1247 Dolman, A. J., Shvidenko, A., Schepaschenko, D., Ciais, P., Tchepakova, N., Chen, T., van der
1248 Molen, M. K., Belelli Marchesini, L., Maximov, T. C., Maksyutov, S., and Schulze, E.-D.:
1249 An estimate of the terrestrial carbon budget of Russia using inventory-based, eddy
1250 covariance and inversion methods, *Biogeosciences*, 9, 5323–5340,
1251 <https://doi.org/10.5194/bg-9-5323-2012>, 2012.
- 1252 Emmons, L. K., Walters, S., Hess, P. G., Lamarque, J.-F., Pfister, G. G., Fillmore, D., Granier,
1253 C., Guenther, A., Kinnison, D., Laepple, T., Orlando, J., Tie, X., Tyndall, G., Wiedinmyer,
1254 C., Baughcum, S. L., and Kloster, S.: Description and evaluation of the Model for Ozone
1255 and Related chemical Tracers, version 4 (MOZART-4), *Geosci. Model Dev.*, 3, 43–67,
1256 <https://doi.org/10.5194/gmd-3-43-2010>, 2010.
- 1257 Enting, I. G., and Newsam, G. N.: Atmospheric constituent inversion problems: Implications
1258 for baseline monitoring, *J. Atmos. Chem.*, 11, 69–87, <https://doi.org/10.1007/BF00053668>,
1259 1990.
- 1260 Feng, S., Jiang, F., Wu, Z., Wang, H., Ju, W., and Wang, H.: CO emissions inferred from surface
1261 CO observations over China in December 2013 and 2017. *Journal of Geophysical Research:*
1262 *Atmospheres*, 125, <https://doi.org/10.1029/2019JD031808>, 2020.
- 1263 [Feng, L., Palmer, P. I., Bösch, H., and Dance, S.: Estimating surface CO₂ fluxes from space-](#)

- 1264 [borne CO₂ dry air mole fraction observations using an ensemble Kalman Filter, Atmos.](#)
1265 [Chem. Phys., 9, 2619–2633, <https://doi.org/10.5194/acp-9-2619-2009>, 2009.](#)
- 1266 [Feng, L., Palmer, P. I., Parker, R. J., Deutscher, N. M., Feist, D. G., Kivi, R., Morino, I., and](#)
1267 [Sussmann, R.: Estimates of European uptake of CO₂ inferred from GOSAT XCO₂ retrievals:](#)
1268 [sensitivity to measurement bias inside and outside Europe. Atmos. Chem. Phys., 16, 1289–](#)
1269 [1302, <https://doi.org/10.5194/acp-16-1289-2016>, 2016.](#)
- 1270 [Feng, L., Palmer, P. I., Bösch, H., Parker, R. J., Webb, A. J., Correia, C. S. C., Deutscher, N. M.,](#)
1271 [Domingues, L. G., Feist, D. G., Gatti, L. V., Gloor, E., Hase, F., Kivi, R., Liu, Y., Miller, J.](#)
1272 [B., Morino, I., Sussmann, R., Strong, K., Uchino, O., Wang, J., and Zahn, A.: Consistent](#)
1273 [regional fluxes of CH₄ and CO₂ inferred from GOSAT proxy XCH₄:XCO₂ retrievals,](#)
1274 [2010–2014, Atmos. Chem. Phys., 17, 4781–4797, <https://doi.org/10.5194/acp-17-4781->](#)
1275 [2017, 2017.](#)
- 1276 Gatti, L. V., Gloor, M., Miller, J. B., Doughty, C. E., Malhi, Y., Domingues, L. G., Basso, L. S.,
1277 Martinewski, A., Correia, C. S. C., Borges, V. F., Freitas, S., Braz, R., Anderson, L. O.,
1278 Rocha, H., Grace, J., Phillips, O. L., and Lloyd, J.: Drought sensitivity of Amazonian carbon
1279 balance revealed by atmospheric measurements. *Nature* 506, 76–80,
1280 <https://doi.org/10.1038/nature12957>, 2014.
- 1281 [Gurney, K. R., Law, R. M., Denning, A. S., Rayner, P. J., Baker, D., Bousquet, P., Bruhwiler,](#)
1282 [L., Chen, Y.-H., Ciais, P., Fan, S., Fung, I. Y., Gloor, M., Heimann, M., Higuchi, K., John,](#)
1283 [J., Maki, T., Maksyutov, S., Masarie, K., Peylin, P., Prather, M., Pak, B. C., Randerson, J.,](#)
1284 [Sarmiento, J., Taguchi, S., Takahashi, T., and Yuen, C.-W.: Towards robust regional esti-](#)
1285 [mates of CO₂ sources and sinks using atmospheric transport models, Nature, 415, 626–630,](#)
1286 <https://doi.org/10.1038/415626a>, 2002.
- 1287 Hayes, D. J., Vargas, R., Alin, S. R., Conant, R. T., Hutyrta, L. R., Jacobson, A. R., Kurz, W. A.,
1288 Liu, S., McGuire, A. D., Poulter, B., and Woodall, C. W.: Chapter 2: The North American
1289 carbon budget. In *Second State of the Carbon Cycle Report (SOCCR2): A Sustained*
1290 *Assessment Report* [Cavallaro, N., G. Shrestha, R. Birdsey, M. A. Mayes, R. G. Najjar, S.
1291 C. Reed, P. Romero-Lankao, and Z. Zhu (eds.)]. U.S. Global Change Research Program,
1292 Washington, DC, USA, pp. 71-108, <https://doi.org/10.7930/SOCCR2.2018.Ch2>, 2018.
- 1293 Hayes, D. J., McGuire, A. D., Kicklighter, D. W., Gurney, K. R., Burnside, T. J., and Melillo, J.
1294 M.: Is the northern high-latitude land-based CO₂ sink weakening?, *Global Biogeochem.*
1295 *Cycles*, 25, GB3018, <https://doi.org/10.1029/2010GB003813>, 2011.
- 1296 He, L., Chen, J., Pisek, J., Schaaf, C.B., and Strahler, A.H.: Global clumping index map derived
1297 from the MODIS BRDF product, *Remote Sens. Environ.*, 119, 118-130,
1298 <https://doi.org/10.1016/j.rse.2011.12.008>, 2012.
- 1299 Houtekamer, P. L., and Mitchell, H. L.: A sequential ensemble Kalman filter for atmospheric
1300 data assimilation, *Monthly Weather Review*, 129(1), 123-137,
1301 [https://doi.org/10.1175/1520-0493\(2001\)129<0123:ASEKFF>2.0.CO;2](https://doi.org/10.1175/1520-0493(2001)129<0123:ASEKFF>2.0.CO;2), 2001.
- 1302 Houweling, S., Baker, D., Basu, S., Boesch, H., Butz, A., Chevallier, F., Deng, F., Dlugokencky,
1303 E. J., Feng, L., Ganshin, A., Hasekamp, O., Jones, D., Maksyutov, S., Marshall, J., Oda, T.,

删除了: Giglio, L., Randerson, J. T., and van der Werf, G. R.: Analysis of daily, monthly, and annual burned area using the fourth-generation global fire emissions database (GFED4) *J. Geophys. Res. Biogeosci.*, 118, 317–328, <https://doi.org/10.1002/jgrg.20042>, 2013.

- 1309 O'Dell, C. W., Oshchepkov, S., Palmer, P. I., Peylin, P., Poussi, Z., Reum, F., Takagi, H.,
 1310 Yoshida, Y., and Zhuravlev, R.: An intercomparison of inverse models for estimating
 1311 sources and sinks of CO₂ using GOSAT measurements, *J. Geophys. Res.-Atmos.*, 120,
 1312 5253–5266, <https://doi.org/10.1002/2014JD022962>, 2015.
- 1313 Hungershofer, K., Breon, F.-M., Peylin, P., Chevallier, F., Rayner, P., Klonecki, A., Houweling,
 1314 S., and Marshall, J.: Evaluation of various observing systems for the global monitoring of
 1315 CO₂ surface fluxes, *Atmos. Chem. Phys.*, 10, 10503–10520, [https://doi.org/10.5194/acp-](https://doi.org/10.5194/acp-10-10503-2010)
 1316 10-10503-2010, 2010.
- 1317 IPCC, 2014: Climate Change 2014: Synthesis Report. Contribution of Working Groups I, II and
 1318 III to the Fifth Assessment Report of the Intergovernmental Panel on Climate Change [Core
 1319 Writing Team, R.K. Pachauri and L.A. Meyer (eds.)]. IPCC, Geneva, Switzerland, 151 pp.
- 1320 Jacobson, A. R., Schuldt, K. N., Miller, J. B., Oda, T., Tans, P., Andrews, A., Mund, J., Ott, L.,
 1321 Collatz, G. J., Aalto, T., Afshar, S., Aikin, K., Aoki, S., Apadula, F., Baier, B., Bergamaschi,
 1322 P., Beyersdorf, A., Biraud, S. C., Bollenbacher, A., Bowling, D., Brailsford, G., Abshire, J.
 1323 B., Chen, G., Chen, H., Chmura, L., Climadat, S., Colomb, A., Conil, S., Cox, A.,
 1324 Cristofanelli, P., Cuevas, E., Curcoll, R., Sloop, C. D., Davis, K., Wekker, S. D., Delmotte,
 1325 M., DiGangi, J. P., Dlugokencky, E., Ehleringer, J., Elkins, J. W., Emmenegger, L., Fischer,
 1326 M. L., Forster, G., Frumau, A., Galkowski, M., Gatti, L. V., Gloor, E., Griffis, T., Hammer,
 1327 S., Haszpra, L., Hatakka, J., Heliasz, M., Hensen, A., Hermanssen, O., Hintsa, E., Holst, J.,
 1328 Jaffé, D., Karion, A., Kawa, S. R., Keeling, R., Keronen, P., Kolari, P., Kominkova, K., Kort,
 1329 E., Krummel, P., Kubistin, D., Labuschagne, C., Langenfelds, R., Laurent, O., Laurila, T.,
 1330 Lauvaux, T., Law, B., Lee, J., Lehner, I., Leuenberger, M., Levin, I., Levula, J., Lin, J.,
 1331 Lindauer, M., Loh, Z., Lopez, M., Lund Myhre, C., Machida, T., Mammarella, I., Manca,
 1332 G., Manning, A., Manning, A., Marek, M. V., Marklund, P., Martin, M. Y., Matsueda, H.,
 1333 McKain, K., Meijer, H., Meinhardt, F., Miles, N., Miller, C. E., Mölder, M., Montzka, S.,
 1334 Moore, F., Morgui, J.-A., Morimoto, S., Munger, B., Necki, J., Newman, S., Nichol, S.,
 1335 Niwa, Y., O'Doherty, S., Ottosson-Löfvenius, M., Paplawsky, B., Peischl, J., Peltola, O.,
 1336 Pichon, J.-M., Piper, S., Plass-Dölmer, C., Ramonet, M., Reyes-Sanchez, E., Richardson,
 1337 S., Riris, H., Ryerson, T., Saito, K., Sargent, M., Sawa, Y., Say, D., Scheeren, B., Schmidt,
 1338 M., Schmidt, A., Schumacher, M., Shepson, P., Shook, M., Stanley, K., Steinbacher, M.,
 1339 Stephens, B., Sweeney, C., Thoning, K., Torn, M., Turnbull, J., Tørseth, K., Bulk, P. V. D.,
 1340 Laan-Luijkx, I. T. V. D., Dinter, D. V., Vermeulen, A., Viner, B., Vitkova, G., Walker, S.,
 1341 Weyrauch, D., Wofsy, S., Worthy, D., Young, D., and Zimnoch, M.: CarbonTracker CT2019,
 1342 <https://doi.org/10.25925/39m3-6069>, 2020.
- 1343 Jiang, F., Wang, H.M., Chen, J.M., Zhou, L.X., Ju, W.M., Ding, A.J., Liu, L.X., and Peters, W.:
 1344 Nested atmospheric inversion for the terrestrial carbon sources and sinks in China,
 1345 *Biogeosciences*, 10(8), 5311–5324, <https://doi.org/10.5194/bg-10-5311-2013>, 2013.
- 1346 Jiang, F., Chen, J. M., Zhou, L. X., Ju, W. M., Zhang, H. F., Machida T., Ciais, P., Peters, W.,
 1347 Wang, H. M., Chen, B. Z., Liu, L. X., Zhang, C. H., Matsueda, H., and Sawa, Y.: A
 1348 comprehensive estimate of recent carbon sinks in China using both top-down and bottom-
 1349 up approaches, *Scientific Reports*, 6, 22130, <https://doi.org/10.1038/srep22130>, 2016.

- 1350 Jin, J., Lin, H. X., Heemink, A., and Segers, A.: Spatially varying parameter estimation for dust
1351 emissions using reduced-tangent-linearization 4DVar, *Atmospheric Environment*, 187, 358-
1352 373, <https://10.1016/j.atmosenv.2018.05.060>, 2018.
- 1353 Ju, W. M., Chen, J. M., Black T. A., Barr A. G., Liu, J., and Chen, B. Z.: Modelling multi-year
1354 coupled carbon and water fluxes in a boreal aspen forest, *Agr. Forest Meteorol.*, 140, 136-
1355 151, <https://doi.org/10.1016/j.agrformet.2006.08.008>, 2006.
- 1356 [Kadyrov, N., Maksyutov, S., Eguchi, N., Aoki, T., Nakazawa, T., Yokota, T., and Inoue, G.:](#)
1357 [Role of simulated GOSAT total column CO₂ observations in surface CO₂ flux uncertainty](#)
1358 [reduction, *J. Geophys. Res.*, 114, D21208, doi:10.1029/2008JD011597, 2009.](#)
- 1359 [Kang, J.-S., Kalnay, E., Miyoshi, T., Liu, J., and Fung, I.:](#) [Estimation of surface carbon fluxes](#)
1360 [with an advanced data assimilation methodology, *J. Geophys. Res.*, 117, D24101,](#)
1361 <https://doi.org/10.1029/2012JD018259>, 2012.
- 1362 Koren, G., Van Schaik, E., Araujo, A.C., Boersma, K.F., Gärtner, A., Killaars, L., Kooreman,
1363 M.L., Kruijt, B., Van der Laan-Luijkx, I.T., Von Randow, C., Smith, N.E., and Peters, W.:
1364 Widespread reduction in sun-induced fluorescence from the Amazon during the 2015/2016
1365 El Niño. *Phil. Trans. R. Soc. B*, 373: 20170408. <http://dx.doi.org/10.1098/rstb.2017.0408>,
1366 2018.
- 1367 Kuze, A., Suto, H., Nakajima, M., and Hamazaki, T.: Thermal and near infrared sensor for
1368 carbon observation Fourier-transform spectrometer on the Greenhouse Gases Observing
1369 Satellite for greenhouse gases monitoring, *Appl. Opt.*, 48, 6716, [https://doi.org/10.1364](https://doi.org/10.1364/AO.48.006716)
1370 [/AO.48.006716](#), 2009.
- 1371 Le Quéré, C., Andrew, R. M., Friedlingstein, P., Sitch, S., Hauck, J., Pongratz, J., Pickers, P. A.,
1372 Ivar Korsbakken, J., Peters, G. P., Canadell, J. G., Armeth, A., Arora, V. K., Barbero, L.,
1373 Bastos, A., Bopp, L., Chevallier, F., Chini, L. P., Ciais, P., Doney, S. C., Gkritzalis, T., Goll,
1374 D. S., Harris, I., Haverd, V., Hoffman, F. M., Hoppema, M., Houghton, R. A., Hurtt, G.,
1375 Ilyina, T., Jain, A. K., Johannesen, T., Jones, C. D., Kato, E., Keeling, R. F., Goldewijk, K.
1376 K., Landschützer, P., Lefèvre, N., Lienert, S., Liu, Z., Lombardozi, D., Metzl, N., Munro,
1377 D. R., Nabel, J. E. M. S., Nakaoka, S., Neill, C., Olsen, A., Ono, T., Patra, P., Pregon, A.,
1378 Peters, W., Peylin, P., Pfeil, B., Pierrot, D., Poulter, B., Rehder, G., Resplandy, L., Robertson,
1379 E., Rocher, M., Rödenbeck, C., Schuster, U., Schwinger, J., Séférian, R., Skjelvan, I.,
1380 Steinhoff, T., Sutton, A., Tans, P. P., Tian, H., Tilbrook, B., N Tubiello, F., van der Laan-
1381 Luijkx, I. T., van der Werf, G. R., Viovy, N., Walker, A. P., Wiltshire, A. J., Wright, R.,
1382 Zaehle, S., and Zheng, B.: Global Carbon Budget 2018, *Earth Syst. Sci. Data*,
1383 <https://doi.org/10.5194/essd-10-2141-2018>, 2018.
- 1384 Liu, Y., Liu, R. G., and Chen, J. M.: Retrospective retrieval of long-term consistent global leaf
1385 area index (1981–2011) from combined AVHRR and MODIS data, *J. Geophys. Res.*, 117,
1386 G04003, <https://doi.org/10.1029/2012JG002084>, 2012.
- 1387 Liu, J., Bowman, K., Parazoo, N. C., Bloom, A A., Wunch, D., Jiang, Z., Gurney, K. R., and
1388 Schimel, D.: Detecting drought impact on terrestrial biosphere carbon fluxes over
1389 contiguous US with satellite observations, *Environmental Research Letters*, 13(9), 095003,

- 1390 <https://doi.org/10.1088/1748-9326/aad5ef>, 2018.
- 1391 Liu, J., Bowman, K. W., Schimel, D. S., Parazoo, N. C., Jiang, Z., Lee, M., Bloom, A. A.,
1392 Wunch, D., Frankenberg, C., Sun, Y., O'Dell, C. W., Gurney, K. R., Menemenlis, D.,
1393 Gierach, M., Crisp, D., and Eldering, A.: Contrasting carbon cycle responses of the tropical
1394 continents to the 2015–2016 El Niño, *Science*, 358, eaam5690,
1395 <https://doi.org/10.1126/science.aam5690>, 2017.
- 1396 Ma, Z. H., Peng, C. H., Zhu, Q., Chen, H., Yu, G. R., Li, W. Z., Zhou, X. L., Wang, W. F., and
1397 Zhang, W. H.: Regional drought-induced reduction in the biomass carbon sink of Canada's
1398 boreal forests, *Proceedings of the National Academy of Sciences*, 109 (7), 2423–2427;
1399 <https://doi.org/10.1073/pnas.1111576109>, 2012.
- 1400 Maksyutov, S., Takagi, H., Valsala, V. K., Saito, M., Oda, T., Saeki, T., Belikov, D. A., Saito,
1401 R., Ito, A., Yo-shida, Y., Morino, I., Uchino, O., Andres, R. J., and Yokota, T.: Regional CO₂
1402 flux estimates for 2009–2010 based on GOSAT and ground-based CO₂ observations, *Atmos.*
1403 *Chem. Phys.*, 13, 9351–9373, <https://doi.org/10.5194/acp-13-9351-2013>, 2013.
- 1404 Miller, C. E., Crisp, D., DeCola, P. L., Olsen, S. C., Randerson, J. T., Michalak, A. M., Alkhaled,
1405 A., Rayner, P., Jacob, D. J., Suntharalingam, P., Jones, D. B. A., Denning, A. S., Nicholls,
1406 M. E., Doney, S. C., Pawson, S., Boesch, H., Connor, B. J., Fung, I. Y., O'Brien, D.,
1407 Salawitch, R. J., Sander, S. P., Sen, B., Tans, P., Toon, G. C., Wennberg, P. O., Wofsy, S. C.,
1408 Yung, Y. L., and Law, R. M.: Precision requirements for space-based XCO₂ data, *J.*
1409 *Geophys. Res.*, 112, D10314, <https://doi.org/10.1029/2006JD007659>, 2007.
- 1410 [Miyazaki, K., Maki, T., Patra, P., and Nakazawa, T.: Assessing the impact of satellite, aircraft,
1411 and surface observations on CO₂ flux estimation using an ensemble-based 4-D data
1412 assimilation system, *J. Geophys. Res.*, 116, D16306, <https://doi.org/10.1029/2010JD015366>, 2011.](https://doi.org/10.1029/2010JD015366)
- 1413
- 1414 Miyazaki, K., Eskes, H. J., Sudo, K., Takigawa, M., van Weele, M., and Boersma, K. F.:
1415 Simultaneous assimilation of satellite NO₂, O₃, CO, and HNO₃ data for the analysis of
1416 tropospheric chemical composition and emissions. *Atmospheric Chemistry and Physics*,
1417 12(20), 9545–9579, <https://doi.org/10.5194/acp-12-9545-2012>, 2012.
- 1418 [Nassar, R., Jones, D. B. A., Kulawik, S. S., Worden, J. R., Bowman, K. W., Andres, R. J.,
1419 Suntharalingam, P., Chen, J. M., Brenninkmeijer, C. A. M., Schuck, T. J., Conway, T. J.,
1420 and Worthy, D. E.: Inverse modeling of CO₂ sources and sinks using satellite observations
1421 of CO₂ from TES and surface flask measurements, *Atmos. Chem. Phys.*, 11, 6029–6047,
1422 <https://doi.org/10.5194/acp-11-6029-2011>, 2011.](https://doi.org/10.5194/acp-11-6029-2011)
- 1423 Nilsson S., Vaganov, E. A., Shvidenko, A., Stolbovoi, V., Rozhkov, V. A., McCallum, I., and
1424 Jonas, M.: Carbon budget of vegetation ecosystems of Russia, *Doklady Earth Sci.*, 363A,
1425 1281–1283, 2003.
- 1426 ObsPack: Cooperative Global Atmospheric Data Integration Project: Multi-laboratory
1427 compilation of atmospheric carbon dioxide data for the period 1957–2018;
1428 obspack_co2_1_GLOBALVIEWplus_v5.0_2019_08_12; NOAA Earth System Research
1429 Laboratory, Global Monitoring Division, <http://dx.doi.org/10.25925/20190812>, 2019.

- 1430 [Oda, T., Maksyutov, S., and Andres, R. J.: The Open-source Data Inventory for Anthropogenic](#)
1431 [CO₂, version 2016 \(ODIAC2016\): a global monthly fossil fuel CO₂ gridded emissions data](#)
1432 [product for tracer transport simulations and surface flux inversions, Earth Syst. Sci. Data,](#)
1433 [10, 87–107, https://doi.org/10.5194/essd-10-87-2018, 2018.](#)
- 1434 O'Dell, C., Connor, B., Bösch, H., O'Brien, D., Frankenberg, C., Castano, R., Christi, M.,
1435 Eldering, D., Fisher, B., Gunson, M., McDuffie, J., Miller, C. E., Natraj, V., Oyafuso, F.,
1436 Polonsky, I., Smyth, M., Taylor, T., Toon, G., Wennberg, P., and Wunch, D.: The ACOS CO₂
1437 retrieval algorithm – Part 1: Description and validation against synthetic observations,
1438 *Atmos. Meas. Tech.*, 5, 99–121, https://doi.org/10.5194/amt-5-99-2012, 2012.
- 1439 Palmer, P. I., Feng, L., Baker, D., Chevallier, F., Bösch, H., and Somkuti, P.: Net carbon
1440 emissions from African biosphere dominate pan-tropical atmospheric CO₂ signal, *Nature*
1441 *communications*, 10, 3344, https://doi.org/10.1038/s41467-019-11097-w, 2019.
- 1442 Pan, Y., Birdsey, R. A., Fang, J., Houghton, R., Kauppi, P. E., Kurz, W. A., Phillips, O. L.,
1443 Shvidenko, A., Lewis, S. L., Canadell, J. G., Ciais, P., Jackson, R. B., Pacala, S., McGuire,
1444 A. D., Piao, S., Rautiainen, A., Sitch, S., and Hayes, D.: A large and persistent carbon sink
1445 in the world's forests, *Science*, 333, 988–993, https://doi.org/10.1126/science.1201609,
1446 2011.
- 1447 Paulo, A. A., Rosa, R. D., and Pereira, L. S.: Climate trends and behavior of drought indices
1448 based on precipitation and evapotranspiration in Portugal, *Nat. Hazards Earth Syst. Sci.*, 12,
1449 1481–1491, https://doi.org/10.5194/nhess-12-1481-2012, 2012.
- 1450 [Peters, W., Miller, J. B., Whitaker, J., Denning, A. S., Hirsch, A., Krol, M. C., Zupanski, D.,](#)
1451 [Bruhwiler, L., and Tans, P. P.: An ensemble data assimilation system to estimate CO₂ surface](#)
1452 [fluxes from atmospheric trace gas observations, J. Geophys. Res., 110, D24304,](#)
1453 [https://doi.org/10.1029/2005JD006157, 2005.](#)
- 1454 Peters, W., Jacobson, A. R., Sweeney, C., Andrews, A. E., Conway, T. J., Masarie, K., Miller, J.
1455 B., Bruhwiler, L. M. P., P'etron, G., Hirsch, A. I., Worthy, D. E. J., Werf, G. R. V. D.,
1456 Randerson, J. T., Wennberg, P. O., Krol, M. C., and Tans, P. P.: An atmospheric perspective
1457 on North American carbon dioxide exchange: CarbonTracker, *P. Natl. Acad. Sci.*, 104,
1458 18925–18930, https://doi.org/10.1073/pnas.0708986104, 2007.
- 1459 Peters, W., Krol, M. C., van der Werf, G. R., Houweling, S., Jones, C. D., Hughes, J., Schaefer,
1460 K., Masarie, K. A., Jacobson, A. R., Miller, J. B., Cho, C. H., Ramonet, M., Schmidt, M.,
1461 Ciattaglia, L., Apadula, F., Helta, D., Meinhardt, F., di Sarra, A. G., Piacentino, S., Sferlazzo,
1462 D., Aalto, T., Hatakka, J., Strom, J., Haszpra, L., Meijer, H. A. J., van der Laan, S., Neubert,
1463 R. E. M., Jordan, A., Rodo, X., Morgui, J. A., Vermeulen, A. T., Popa, E., Rozanski, K.,
1464 Zimnoch, M., Manning, A. C., Leuenberger, M., Uglietti, C., Dolman, A. J., Ciais, P.,
1465 Heimann, M., and Tans, P. P.: Seven years of recent European net terrestrial carbon dioxide
1466 exchange constrained by atmospheric observations, *Glob. Change Biol.*, 16, 1317–1337,
1467 https://doi.org/10.1111/j.1365-2486.2009.02078.x, 2010.
- 1468 Peylin, P., Law, R. M., Gurney, K. R., Chevallier, F., Jacobson, A. R., Maki, T., Niwa, Y., Patra,
1469 P. K., Peters, W., Rayner, P. J., Rödenbeck, C., van der Laan-Luijkx, I. T., and Zhang, X.:

删除了: Oda, T. and Maksyutov, S.: A very high-resolution (1 km x 1 km) global fossil fuel CO₂ emission inventory derived using a point source database and satellite observations of nighttime lights. *Atmos. Chem. Phys.* 11, 543–556, https://doi.org/10.5194/acp-11-543-2011, 2011.

- 1475 Global atmospheric carbon budget: results from an ensemble of atmospheric CO₂ inversions,
1476 *Biogeosciences*, 10, 6699–6720, <https://doi.org/10.5194/bg-10-6699-2013>, 2013.
- 1477 Phillips, O. L., Aragao, L., Lewis, S. L., Fisher, J. B., Lloyd, J., Lopez-Gonzalez, G., Malhi, Y.,
1478 Monteagudo, A., Peacock, J., Quesada, C. A., van der Heijden, G., Almeida, S., Amaral, I.,
1479 Arroyo, L., Aymard, G., Baker, T. R., Banki, O., Blanc, L., Bonal, D., Brando, P., Chave, J.,
1480 de Oliveira, A. C. A., Cardozo, N. D., Czimczik, C. I., Feldpausch, T. R., Freitas, M. A.,
1481 Gloor, E., Higuchi, N., Jimenez, E., Lloyd, G., Meir, P., Mendoza, C., Morel, A., Neill, D.
1482 A., Nepstad, D., Patino, S., Penuela, M. C., Prieto, A., Ramirez, F., Schwarz, M., Silva, J.,
1483 Silveira, M., Thomas, A. S., ter Steege, H., Stropp, J., Vasquez, R., Zelazowski, P., Davila,
1484 E. A., Andelman, S., Andrade, A., Chao, K. J., Erwin, T., Di Fiore, A., Honorio, E., Keeling,
1485 H., Killeen, T. J., Laurance, W. F., Cruz, A. P., Pitman, N. C. A., Vargas, P. N., Ramirez-
1486 Angulo, H., Rudas, A., Salamao, R., Silva, N., Terborgh, J., and Torres-Lezama, A.: Drought
1487 sensitivity of the Amazon forest, *Science*, 323, 1344–1347, [https://doi.org/](https://doi.org/10.1126/science.1164033)
1488 [10.1126/science.1164033](https://doi.org/10.1126/science.1164033), 2009.
- 1489 [Piao, S., Wang, X., Wang, K., Li, X., Bastos, A., Canadell, J. G., Ciais, P., Friedlingstein, P.,
1490 and Sitch, S.: Interannual variation of terrestrial carbon cycle: Issues and perspectives, *Glob
1491 Change Biol.*, 26, 300–318, <https://doi.org/10.1111/gcb.14884>, 2020.](https://doi.org/10.1111/gcb.14884)
- 1492 Rödenbeck, C.: Estimating CO₂ sources and sinks from atmospheric mixing ratio
1493 measurements using a global inversion of atmospheric transport, Technical Report 6, Max
1494 Planck Institute for Biogeochemistry, Jena, 2005.
- 1495 [Randerson, J.T., van der Werf, G.R., Giglio, L., Collatz, G.J., and Kasibhatla, P.S.: Global Fire
1496 Emissions Database, Version 4.1 \(GFEDv4\). ORNL DAAC, Oak Ridge, Tennessee, USA.
1497 <https://doi.org/10.3334/ORNLDAAC/1293>, 2017.](https://doi.org/10.3334/ORNLDAAC/1293)
- 1498 Saeki, T., Maksyutov, S., Saito, M., Valsala, V., Oda, T., Andres, R. J., Belikov, D., Tans, P.,
1499 Dlugokencky, E., Yoshida, Y., Morino, I., Uchino, O., and Yokota, T.: Inverse modeling of
1500 CO₂ fluxes using GOSAT data and multi-year ground-based observations, *SOLA*, 9, 45–50,
1501 <https://doi.org/10.2151/sola.2013-011>, 2013a.
- 1502 Saeki, T., Maksyutov, S., Sasakawa, M., Machida, T., Arshinov, M., Tans, P., Conway, T. J.,
1503 Saito, M., Valsala, V., Oda, T., Andres, R. J., and Belikov, D.: Carbon flux estimation for
1504 Siberia by inverse modeling constrained by aircraft and tower CO₂ measurements, *J.
1505 Geophys. Res. Atmos.*, 118, 1100–1122, <https://doi.org/10.1002/jgrd.50127>, 2013b.
- 1506 Scholze, M., Kaminski, T., Knorr, W., Voßbeck, M., Wu, M., Ferrazzoli, P., Kerr, Y., Mialon,
1507 A., Richaume P., Rodríguez-Fernández, N., Vittucci, C., Wigneron, J.-P., Mecklenburg, S.,
1508 and Drusch, M.: Mean European carbon sink over 2010–2015 estimated by simultaneous
1509 assimilation of atmospheric CO₂, soil moisture, and vegetation optical depth. *Geophysical
1510 Research Letters*, 46, 13796–13803, <https://doi.org/10.1029/2019GL085725>, 2019.
- 1511 Takagi, H., Saeki, T., Oda, T., Saito, M., Valsala, V., Belikov, D., Saito, R., Yoshida, Y., Morino,
1512 I., Uchino, O., Andres, R. J., Yokota, T., and Maksyutov, S.: On the Benefit of GOSAT
1513 Observations to the Estimation of Regional CO₂ Fluxes, *SOLA*, 7, 161–164,
1514 <https://doi.org/10.2151/sola.2011-041>, 2011.

1515 Takahashi, T., Sutherland, S. C., Wanninkhof, R., Sweeney, C., Feely, R. A., Chipman, D. W.,
1516 Hales, B., Friederich, G., Chavez, F., Sabine, C., Watson, A., Bakker, D. C. E., Schuster, U.,
1517 Metzl, N., Yoshikawa-Inoue, H., Ishii, M., Midorikawa, T., Nojiri, Y., Körtzinger, A.,
1518 Steinhoff, T., Hoppema, M., Olafsson, J., Arnarson, T. S., Tilbrook, B., Johannessen, T.,
1519 Olsen, A., Bellerby, R., Wong, C. S., Delille, B., Bates, N. R., and de Baar, H. J. W.:
1520 Climatological mean and decadal change in surface ocean pCO₂, and net sea-air CO₂ flux
1521 over the global oceans. *Deep Sea Research Part II: Topical Studies in Oceanography*, 56 (8-
1522 10): 554-577, <https://doi.org/10.1016/j.dsr2.2008.12.009>, 2009.

1523 van der Laan-Luijkx, I. T., van der Velde, I. R., Krol, M. C., Gatti, L. V., Domingues, L. G.,
1524 Correia, C. S. C., Miller, J. B., Gloor, M., van Leeuwen, T. T., Kaiser, J. W., Wiedinmyer,
1525 C., Basu, S., Clerbaux, C., and Peters, W.: Response of the Amazon carbon balance to the
1526 2010 drought derived with CarbonTracker South America, *Global Biogeochem. Cycles*, 29,
1527 1092–1108, <https://doi.org/10.1002/2014GB005082>, 2015.

1528 Vicente-Serrano, S. M., Gouveia, C., Camarero, J. J., Beguería, S., Trigo, R., López-Moreno, J.
1529 I., Azorín-Molina, C., Pasho, E., Lorenzo-Lacruz, J., Revuelto, J., and Morán-Tejeda, E.:
1530 Response of vegetation to drought time-scales across global land biomes, *P. Natl. Acad. Sci.*
1531 USA., 110, 52–57, <https://doi.org/10.1073/pnas.1207068110>, 2013.

1532 Wang, H. M., Jiang, F., Wang, J., Ju, W. M., and Chen, J. M.: Terrestrial ecosystem carbon flux
1533 estimated using GOSAT and OCO-2 XCO₂ retrievals, *Atmos. Chem. Phys.*, 19, 12067–
1534 12082, <https://doi.org/10.5194/acp-19-12067-2019>, 2019.

1535 Wang, J., Zeng, N., Wang, M. R., Jiang, F., Wang, H. M., and Jiang, Z. Q.: Contrasting terrestrial
1536 carbon cycle responses to the 1997/98 and 2015/16 extreme El Niño events, *Earth System*
1537 *Dynamics*, 9, 1–14, <https://doi.org/10.5194/esd-9-1-2018>, 2018**.**

1538 Wang, J. S., Kawa, S. R., Collatz, G. J., Sasakawa, M., Gatti, L. V., Machida, T., Liu, Y., and
1539 Manyin, M. E.: A global synthesis inversion analysis of recent variability in CO₂ fluxes
1540 using GOSAT and in situ observations, *Atmos. Chem. Phys.*, 18, 11097–11124,
1541 <https://doi.org/10.5194/acp-18-11097-2018>, 2018**a.**

1542 Whitaker, J. S., and Hamill, T. M.: Ensemble data assimilation without perturbed observations.
1543 *Monthly Weather Review*, 130(7), 1913-1924. [https://10.1175/1520-0493\(2002\)130<1913:Edawpo>2.0.Co;2](https://10.1175/1520-0493(2002)130<1913:Edawpo>2.0.Co;2), 2002.

1545 Wolf, S., Keenan, T. F., Fisher, J. B., Baldocchi, D. D., Desai, A. R., Richardson, A. D., Scott,
1546 R. L., Law, B. E., Litvak, M. E., Brunzell, N. A., Peters, W., and van der Laan-Luijkx, I. T.,
1547 Warm spring reduced carbon cycle impact of the 2012 US summer drought, *Proceedings of*
1548 *the National Academy of Sciences*, 113 (21) 5880-5885;
1549 <https://doi.org/10.1073/pnas.1519620113>, 2016.

1550 Wunch, D., Wennberg, P. O., Toon, G. C., Connor, B. J., Fisher, B., Osterman, G. B.,
1551 Frankenberg, C., Man-drake, L., O'Dell, C., Ahonen, P., Biraud, S. C., Castano, R., Cressie,
1552 N., Crisp, D., Deutscher, N. M., Eldering, A., Fisher, M. L., Griffith, D. W. T., Gunson, M.,
1553 Heikkinen, P., Keppel-Aleks, G., Kyrö, E., Lindenmaier, R., Macatangay, R., Mendonca, J.,
1554 Messerschmidt, J., Miller, C. E., Morino, I., Notholt, J., Oyafuso, F. A., Rettinger, M.,

删除了: van der Werf, G. R., Randerson, J. T., Giglio, L., Collatz, G. J., Mu, M., Kasibhatla, P. S., Morton, D. C., DeFries, R. S., Jin, Y., and van Leeuwen, T. T.: Global fire emissions and the contribution of deforestation, savanna, forest, agricultural, and peat fires (1997–2009), *Atmos. Chem. Phys.*, 10, 11707–11735, <https://doi.org/10.5194/acp-10-11707-2010>, 2010.

1562 Robinson, J., Roehl, C. M., Salawitch, R. J., Sherlock, V., Strong, K., Sussmann, R., Tanaka,
1563 T., Thompson, D. R., Uchino, O., Warneke, T., and Wofsy, S. C.: A method for evaluating
1564 bias in global measurements of CO₂ total columns from space, *Atmos. Chem. Phys.*, 11,
1565 12317–12337, <https://doi.org/10.5194/acp-11-12317-2011>, 2011.

1566 Zamolodchikov, D.G., Grabovskii, V.I., Shulyak, P.P., and Chestnykh, O. V.: Recent decrease
1567 in carbon sink to Russian forests, *Doklady Biological Sciences*, 476, 200–202,
1568 <https://doi.org/10.1134/S0012496617050064>, 2017.

1569 Zhang, S., Zheng, X., Chen, J. M., Chen, Z., Dan, B., Yi, X., Wang, L., and Wu, G.: A global
1570 carbon assimilation system using a modified ensemble Kalman filter, *Geosci. Model Dev.*,
1571 8, 805–816, <https://doi.org/10.5194/gmd-8-805-2015>, 2015.

1572 Zhao, M. S., and Running, S. W.: Drought-Induced Reduction in Global Terrestrial Net Primary
1573 Production from 2000 Through 2009, *Science*, 329, 940–943,
1574 <https://doi.org/10.1126/science.1192666>, 2010.

1575 Zhang, H. F., Chen, B. Z., van der Laan-Luijk, I. T., Machida, T., Matsueda, H., Sawa, Y.,
1576 Fukuyama, Y., Langenfelds, R., van der Schoot, M., Xu, G., Yan, J. W., Cheng, M. L., Zhou,
1577 L. X., Tans, P. P., and Peters, W.: Estimating Asian terrestrial carbon fluxes from
1578 CONTRAIL aircraft and surface CO₂ observations for the period 2006–2010, *Atmos. Chem.*
1579 *Phys.*, 14, 5807–5824, <https://doi.org/10.5194/acp-14-5807-2014>, 2014.

1580 Zhu, Z., Bi, J., Pan, Y., Ganguly, S., Anav, A., Xu, L., Samanta, A., Piao, S., Nemani, R.R., and
1581 Myneni, R. B.: Global Data Sets of Vegetation Leaf Area Index (LAI)_{3g} and Fraction of
1582 Photosynthetically Active Radiation (FPAR)_{3g} Derived from Global Inventory Modeling
1583 and Mapping Studies (GIMMS) Normalized Difference Vegetation Index (NDVI_{3g}) for the
1584 Period 1981 to 2011, *Remote Sensing*, 5, 927–948, <https://doi.org/10.3390/rs5020927>, 2013.

1585